Volume 4 OCTOBER, 1933 Number 10

PHYSICS

A Journal of General and Applied Physics

The Measurement of Heat Production in Diathermy

ALLAN HEMINGWAY AND J. F. MCCLENDON, *Laboratory of Physiological Chemistry, The Medical School, University of Minnesota*

(Received June 12, 1933)

Resistance and reactance of diathermy patients to alternating currents of varying frequencies up to and including radiofrequencies have been measured with a high frequency Wheatstone bridge. At frequencies greater than one million cycles per second the resistance becomes constant and the reactance and phase angle decrease to zero. Under these conditions the human body behaves as a pure resistance and the heat production in calories can be computed from the formula $0.24\ VIt$ where V is the root-mean-square voltage, I the root-mean-square current and t the duration time in seconds of the diathermy treatment. High frequency resistances of various parts of the body which are usually treated with diathermy are given.

IN medical diathermy a high frequency alternating current passes between electrodes applied to the skin of the patient and heat is generated in the tissues traversed by the current. The frequency of the alternating current is sufficiently great to prevent electrical stimulation of the neuromuscular system. In physiological problems related to temperature-control and water-balance it is desired to measure the total amount of heat imparted to an animal or to a patient during a diathermy treatment. It is obvious that calorimetric measurements of this quantity would be extremely involved. A simple method would be to measure the high frequency current and high frequency voltage and, if the phase angle were known, it would be possible to compute the heat production from these quantities. The present paper is concerned with a measurement of the electrical resistance and reactance of the patient during a diathermy treatment at frequencies up to and including diathermy frequencies. Knowing the resistance and reactance at various frequencies it is possible to compute the phase angle.

There is evidence that the phase angle of biological tissues decreases to a low value at radiofrequencies. Philippson[1] found by measuring impedance of tissues at various frequencies that the impedance became constant for values of the frequency greater than one million cycles per second. Fricke[2] measured the resistance and capacity of red cell suspensions at various frequencies and found that the resistance decreased to a low constant value between one and ten million cycles per second. This constancy of the resistance at high frequency indicates that the phase angle is small at high frequency. McClendon[3, 4] observed a large decrease of resistance of red cell suspension as the frequency of the a.c. current used to measure resistance increased. Hemingway[5] in calorimetric determinations of the heat production by diathermy currents in vegetable tissue found that the phase angle of the diathermy current was very small.

Measurements of resistance and capacity were

[1] Philippson, Comptes Rendus Soc. Biol. **83**, 287 (1920).
[2] Fricke, J. Gen. Physiol. **9**, 153 (1925).
[3] McClendon, J. Biol. Chem. **69**, 733 (1926).
[4] McClendon, Am. J. Physiol. **82**, 525 (1927).
[5] Hemingway, Radiology **17**, 136 (1931).

made on the high frequency Wheatstone bridge described in a previous paper by Hemingway and McClendon.[6] Additional coils and capacities have been inserted into the oscillating circuits and the detector circuit, in order to measure resistances and reactances with alternating currents at frequencies from the audiorange of frequencies upwards. In order to eliminate the use of an extremely high capacity at lower frequencies, the arrangement of the balancing arm of the bridge was a variable high frequency resistor in parallel with a variable air-mica condenser. The corresponding series resistances and capacities were computed from the observed parallel resistances and capacities by the well-known formulas

$$\text{Series resistance} = R/(1+S^2) \text{ ohms},$$

$$\text{Series reactance} = RS/(1+S^2) \text{ ohms},$$

where R is the observed parallel resistance, C is the observed parallel capacity, f is the frequency of the alternating current and $S = 2\pi fRC$.

Measurements of resistance and capacity were made with alternating currents of frequencies from 1000 cycles per second to 1.5×10^6 cycles per second. The resulting series resistances and reactances of the tissues with electrodes at various parts of the body are given in Fig. 1. It is to be observed that, as the frequency of the alternating current increased, the reactance decreased and approached zero in the range of frequencies which include diathermy alternating currents. In this range the resistance approached a constant value. Hence, in this diathermy range of frequencies the phase angle approaches zero.

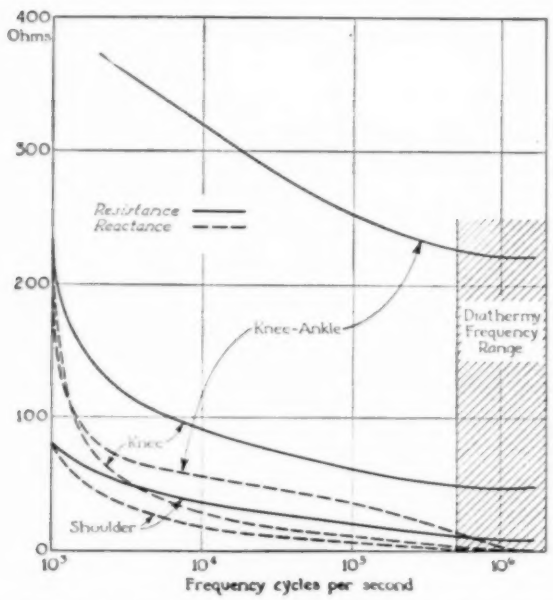

FIG. 1. Variation of diathermy resistance and reactance with frequency.

[6] Hemingway and McClendon, Physics **2**, 396 (1932).

Only three representative curves showing the variation of reactance with resistance are given. Others have a similar shape but have been omitted to prevent confusion because of too many curves on a single graph. The knee-ankle resistance and reactance values were obtained from a cuff electrode above the knee and an electrode below the sole of the foot, which was immersed in salt solution. For the knee, cuff electrodes above and below the knee were used. For the shoulder, two 9×16 cm² electrodes were used, one anterior, the other posterior. The following table contains values of the high frequency resistance of patients measured with alternating current of 1.5 million cycles per second, together with the type and size of the diathermy electrode applied.

TABLE I.

Region treated	Electrode	Resistance (ohms)
Shoulder	Metal 9×16 cm²	37
Shoulder	Metal 9×16 cm²	28
Shoulder	Metal 9×16 cm²	40
Sacro-iliac	Metal 9×16 cm² (back) / Metal 17×17 cm² (front)	34
Knee	Pad 9×16 cm²	40
Knee	Pad 9×16 cm²	50
Ankle (calf to sole)	Cuff and pad	150

DISCUSSION OF RESULTS

The curves of reactance and resistance *vs.* frequency show that as the diathermy range of frequencies is approached the phase angle, i.e., arctan (X/R) where X is the series reactance and R is the resistance, becomes zero. The heat production in calories is given by the expression $0.24\ VIt\cos\theta$ where V is the root-mean-square voltage and I the root-mean-square current and t the time in seconds. Since θ is zero, or very close to zero, the value of the heat production in calories during a time of t seconds becomes $0.24\ VIt$. This shows that the human body behaves

to diathermy current as a pure resistance and the heat production can be computed from the observed voltage and current values.

Diathermy machines are equipped with a meter which indicates the root-mean-square current and in machines examined and tested it has been found that the meters are quite accurate. The measurement of the root-mean-square high frequency voltage presents certain difficulties in regard to balanced shielding and elimination of stray currents. The Weston Instrument Company have recently designed two voltmeters on the thermocouple principle for the purpose of measuring high frequency diathermy voltage, which have proved satisfactory. Full scale deflections of these instruments are 50 and 125 volts and measurement of heat production in animal tissues during diathermy treatments is being carried on with the use of these instruments.

One of these instruments was purchased with a grant from the American Medical Association and we wish to take this occasion to thank the Association and Mr. H. A. Carter, Secretary of the Council of Physical Therapy, for this assistance.

Note on Dipole Radiation Theory

W. Howard Wise, *American Telephone and Telegraph Company, New York*

(Received June 17, 1933)

By fitting certain general asymptotic series solutions of the wave equation to known expressions for wave function components at the surface of the ground and on the upper infinite hemisphere, recurrence relations between the successive terms of the asymptotic series for some of the dipole wave function components are obtained.

Introduction

PAST attempts to calculate the radiation field of a dipole on or near a flat homogeneous earth have been chiefly confined to efforts at direct evaluation of the Sommerfeld and von Hoerschelmann infinite integral representations of dipole wave functions. Because of the great complexity of these integrals this direct attack has failed to yield an explicit recurrence relation for any of the wave function component series in the air. However, in the case of the vertical dipole of zero height, centered on the interface between air and ground, rigorous series expansions, both convergent and asymptotic, which hold at the surface of the ground, have been derived for each of the wave function components[1] and the first term of the asymptotic expansion for the sky wave from any dipole is known.[2] In these cases where we have rigorous expressions for wave function components on the boundaries of the air (the surface of the flat earth and the upper infinite hemisphere) the problem may be regarded as one of finding the solutions of the wave equation in air which reduce to these expressions on the boundaries. In this paper recurrence relations for two of the wave function component series are obtained by fitting appropriate asymptotic series solutions of the wave equation to two of the known expressions for these wave function components on the boundaries of the air. The solutions of the wave equation assumed for this purpose appear to be new.

A Recurrence Relation for Q_1

In the air, the wave function for a dipole in air is a solution of the wave equation $\nabla^2 W + k_1^2 W = 0$. The primary wave function is the simple solution $\exp(ik_1 r)/r$. The whole wave function is $u + \exp(ik_1 r)/r$, where u is the wave function for the currents in the ground. Then $\nabla^2 u + k_1^2 u = 0$.

Sommerfeld has shown that u may be conveniently separated into three component parts, $u = P + Q_1 + Q_2$, of which P is the Zenneck wave or ground wave which is completely known and so not considered here, Q_1 is a spherical wave and Q_2 is a highly attenuated, and therefore for most purposes relatively insignificant, wave of hybrid character.

In polar coordinates (see Fig. 1) $\nabla^2 u + k_1^2 u = 0$ is

$$\frac{1}{r_2^2}\frac{\partial}{\partial r_2} r_2^2 \frac{\partial u}{\partial r_2} + \frac{1}{r_2^2 \sin\theta}\frac{\partial}{\partial \theta} \sin\theta \frac{\partial u}{\partial \theta} + \frac{1}{r_2^2 \sin^2\theta}\frac{\partial^2 u}{\partial \phi^2} + k_1^2 u = 0.$$

Writing $ik_1 r_2 = \bar{\omega}$ and $\cos\theta = c$ this takes the somewhat simpler form

$$\frac{1}{\bar{\omega}^2}\frac{\partial}{\partial \bar{\omega}} \bar{\omega}^2 \frac{\partial u}{\partial \bar{\omega}} + \frac{1}{\bar{\omega}^2}\frac{\partial}{\partial c}(1-c^2)\frac{\partial u}{\partial c} + \frac{1}{\bar{\omega}^2(1-c^2)}\frac{\partial^2 u}{\partial \phi^2} - u = 0. \tag{1}$$

[1] W. H. Wise, Proc. I. R. E. **19**, 1684 (1931).

[2] W. H. Wise, Bell Sys. Tech. J. **8**, 662 (1929).

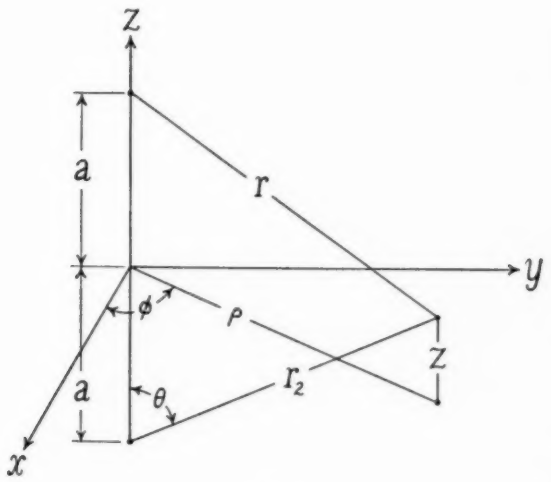

FIG. 1.

Assuming a solution of the form

$$Q_1 = ik_1 \cos m(\phi-\phi_0)\sum_{n=1}^{\infty} \frac{e^{\tilde{\omega}}}{\tilde{\omega}^n} g_{mn}(c) \tag{2}$$

one gets

$$ik_1 \cos m(\phi-\phi_0)\sum_{n=1}^{\infty} \frac{e^{\tilde{\omega}}}{\tilde{\omega}^{n+2}}\left\{(1-c^2)g_{mn}''(c)-2cg_{mn}'(c)+\left[n(n-1)-\frac{m^2}{1-c^2}\right]g_{mn}(c)-2ng_{m(n+1)}(c)\right\}=0,$$

whence

$$g_{m(n+1)}(c)=\left(\frac{n-1}{2}-\frac{m^2}{(1-c^2)2n}\right)g_{mn}(c)-\frac{c}{n}g_{mn}'(c)+\frac{1-c^2}{2n}g_{mn}''(c). \tag{3}$$

This is as would be suspected; since the first term of the asymptotic Q_1-component series (2) is Q_1 on the sphere at infinity, a knowledge of it alone serves to completely determine Q_1.

Parenthetically, it may be remarked that the series (2) must be Q_1 and not the complete solution because P and Q_2 are exponentially attenuated and a series of this character cannot represent an exponentially attenuated function.

In the case of the vertical dipole we know by previous work,[2] and also by reciprocity, that the first term of Q_1 is $R_1 \exp ik_1r_2/r_2$, where R_1 is the coefficient of reflection for a plane, electromagnetic wave polarized with the electric vector in the plane of incidence. Hence, in this case, m is zero and

$$g_{01}(c)=R_1=\frac{c-\eta\tau(1-\tau^2(1-c^2))^{\frac{1}{2}}}{c+\eta\tau(1-\tau^2(1-c^2))^{\frac{1}{2}}},$$

where $\eta=\mu_2/\mu_1$, $\tau=k_1/k_2$ and

$$k^2=\epsilon\mu\omega^2+4\pi\omega\sigma\mu i\omega=k_1^2 \text{ in the air } (k_1\approx 2\pi/\lambda)$$
$$=k_2^2 \text{ in the ground.}$$

In the case of the horizontal dipole we know by previous work[2] that the first term of Q_1 is the vector

$$a\times\frac{\tau c-(1-\tau^2(1-c^2))^{\frac{1}{2}}}{\tau c+(1-\tau^2(1-c^2))^{\frac{1}{2}}}\cdot\frac{e^{ik_1r_2}}{r_2}+b\times 0+c\times\frac{-2\cos\phi\cdot\tau(1-\tau^2)c(1-c^2)^{\frac{1}{2}}}{(\tau c+(1-\tau^2(1-c^2))^{\frac{1}{2}})\cdot(c+\tau(1-\tau^2(1-c^2))^{\frac{1}{2}})}\cdot\frac{e^{ik_1r_2}}{r_2},$$

where the a, b and c preceding the multiplication signs are unit vectors pointing in the x, y and z directions. The earth permeability has been assumed to be unity. The dipole points in the positive x-direction. Clearly, the x-component of Q_1 is defined by $m=0$ and

$$g_{01}(c)=\frac{\tau c-(1-\tau^2(1-c^2))^{\frac{1}{2}}}{\tau c+(1-\tau^2(1-c^2))^{\frac{1}{2}}};$$

while the z-component of Q_1 is defined by $m=1$, $\phi_0=0$ and

$$g_{11}(c)=\frac{-\tau(1-\tau^2)c(1-c^2)^{\frac{1}{2}}}{(\tau c+(1-\tau^2(1-c^2))^{\frac{1}{2}})\cdot(c+\tau(1-\tau^2(1-c^2))^{\frac{1}{2}})}.$$

A Transformation of the Series (2)

Since the solution of the wave equation in polar coordinates as usually derived is a series of products of Hankel functions and associated Legendre functions, it is natural to seek to identify the series (2) with the ordinary formal solution. The ordinary type of solution appropriate for the representation of Q_1 is

$$Q_1=ik_1\cos m(\phi-\phi_0)\sum_{n=0}^{\infty}A_n i^n\left(\frac{\pi}{2k_1r_2}\right)^{\frac{1}{2}}H^{(1)}_{n+\frac{1}{2}}(k_1r_2)P_n^m(c) \tag{4}$$

$$=ik_1\cos m(\phi-\phi_0)\left[A_0\frac{e^{\tilde{\omega}}}{\tilde{\omega}}P_0^m(c)+A_1\frac{e^{\tilde{\omega}}}{\tilde{\omega}}\left(1-\frac{1}{\tilde{\omega}}\right)P_1^m(c)+\cdots\right]$$

$$=ik_1\cos m(\phi-\phi_0)\left[\frac{e^{\tilde{\omega}}}{\tilde{\omega}}\sum_0^{\infty}A_nP_n^m(c)+\frac{e^{\tilde{\omega}}}{\tilde{\omega}^2}\sum_1^{\infty}-\frac{n(n+1)}{2\times1!}A_nP_n^m(c)\right.$$

$$\left.+\frac{e^{\tilde{\omega}}}{\tilde{\omega}^3}\sum_2^{\infty}\frac{(n-1)n(n+1)(n+2)}{2^2\times2!}A_nP_n^m(c)+\cdots\right].$$

Now

$$\left(\frac{s-1}{2}-\frac{m^2}{(1-c^2)2s}\right)P_n^m(c)-\frac{c}{s}\frac{d}{dc}P_n^m(c)+\frac{1-c^2}{2s}\frac{d^2}{dc^2}P_n^m(c)$$

$$=\frac{1}{2s}\left[(1-c^2)\frac{d^2}{dc^2}P_n^m(c)-2c\frac{d}{dc}P_n^m(c)+\left\{s(s-1)-\frac{m^2}{1-c^2}\right\}P_n^m(c)\right]$$

$$=\frac{1}{2s}[s(s-1)-n(n+1)]P_n^m(c)=-\frac{(n+1-s)(n+s)}{2s}P_n^m(c). \tag{5}$$

It follows that, if $g_{m1}(c)=\sum_0^{\infty}A_nP_n^m(c)$ then,

$$g_{m2}(c)=\sum_1^{\infty}-\frac{n(n+1)}{2\times1!}A_nP_n^m(c);\qquad g_{m3}(c)=\sum_2^{\infty}\frac{(n-1)n(n+1)(n+2)}{2^2\times2!}A_nP_n^m(c),\ \cdots.$$

Hence the two solutions are identical if the constants A_n are defined by

$$A_n=\frac{2n+1}{2}\cdot\frac{(n-m)!}{(n+m)!}\int_{-1}^{1}g_{m1}(c)P_n^m(c)dc. \tag{6}$$

$g_{01}(c)$ is only defined for positive values of c; for negative values of c it is at our disposal. In the case of the vertical dipole the integration can be effected without much trouble. Since $P_n(c)$ is a polynomial in c the chief problem is the evaluation of the integral

$$I_n = \int_0^1 g_{01}(c) c^n dc. \tag{7}$$

The integration is straightforward but a bit long.

If $g_{01}(-c) = -2 - g_{01}(c)$ and $\tau = 1/4$ then

$$A_0 = -1, \quad A_2 = A_4 = A_6 = \cdots = 0,$$
$$A_1 = +2.1137, \quad A_3 = -0.7795, \quad A_5 = +0.4274,$$
$$A_7 = -0.2689, \quad A_9 = +0.1829, \quad A_{11} = -0.1311, \quad \cdots.$$

So, at least for this particular choice of $g_{01}(-c)$, the series (4) is rather slowly convergent.

An unfortunate property of the $g_{01}(-c)$ chosen is that while it makes $g_{01}(c)$ and its first derivative continuous at $c = 0$ it also makes the second derivative and so also $g_{02}(c)$, discontinuous at $c = 0$. This is a difficulty which it is not easy to avoid.

A Recurrence Relation for Q_2

It has already been found that at the surface of the ground the Q_2 component of the wave function for a vertical dipole of zero height is[1]

$$Q_2 \sim \frac{ik_1\tau}{1-\tau^2} \cdot \frac{e^\eta}{\eta} \left(\frac{D_1}{\eta} + \frac{D_2}{\eta^2} + \frac{D_3}{\eta^3} + \cdots \right), \tag{8}$$

where $\eta = ik_2\rho$, $D_1 = (1+\tau^2)$, $D_2 = 3(1+\tau^2)^2 - (1+\tau^2)$ and $D_n = (1+\tau^2)[(2n-1)D_{n-1} - (n-1)^2 D_{n-2}]$.

We seek a solution of the wave equation which will reduce to (10) at the surface of the ground. To this end we assume the asymptotic solution form (9),

$$Q_2 \sim \frac{ik_1\tau}{1-\tau^2} \cdot \frac{e^\eta}{\eta} \left(\frac{D_1}{\eta}\phi_1(\zeta) + \frac{D_2}{\eta^2}\phi_2(\zeta) + \cdots \right), \tag{9}$$

where $\zeta = k_2 z$, substitute (9) into the wave equation in cylindrical coordinates, equate to zero the coefficient of each power of $1/\eta$, solve the resulting sequence of differential equation in the $\phi_n(\zeta)$ and apply the boundary conditions $\phi_n(0) = 1$, $\phi_n(\infty) = 0$.

The differential equations to be solved are

$$\phi_1''(\zeta) - (1-\tau^2)\phi_1(\zeta) = 0$$
$$D_2[\phi_2''(\zeta) - (1-\tau^2)\phi_2(\zeta)] = -3D_1\phi_1(\zeta),$$
$$D_3[\phi_3''(\zeta) - (1-\tau^2)\phi_3(\zeta)] = -5D_2\phi_2(\zeta) + 2^2 D_1\phi_1(\zeta),$$
$$\cdots\cdots\cdots\cdots\cdots\cdots\cdots\cdots\cdots\cdots\cdots\cdots\cdots\cdots\cdots\cdots\cdots\cdots$$
$$D_n[\phi_n''(\zeta) - (1-\tau^2)\phi_n(\zeta)] = -(2n-1)D_{n-1}\phi_{n-1}(\zeta) + (n-1)^2 D_{n-2}\phi_{n-2}(\zeta).$$

It is easy to solve a few of these equations but, after the third, the labor required soon reaches prohibitive proportions. The solutions of the first two equations are

$$\phi_1(\zeta) = e^{-\zeta(1-\tau^2)^{\frac{1}{2}}}; \qquad \phi_2(\zeta) = \left(1 + \frac{3D_1}{D_2} \cdot \frac{\zeta}{2(1-\tau^2)^{\frac{1}{2}}}\right) e^{-\zeta(1-\tau^2)^{\frac{1}{2}}}.$$

If a $D_0\phi_0(\zeta)$ term is added to (9) it turns out that $\phi_0(\zeta)=0$.

The Q_2 just derived is the Q_2 for the integral

$$\frac{1+\tau^2}{2}\int_{-\infty}^{\infty}\frac{1}{l+\tau^2 m}H_0^{(1)}(\lambda\rho)e^{-zl}\lambda d\lambda,$$

where $l=(\lambda^2-k_1^2)^{\frac{1}{2}}$ and $m=(\lambda^2-k_2^2)^{\frac{1}{2}}$, the wave function for a vertical dipole of zero height.

If the vertical dipole is of finite height its wave function is

$$\frac{e^{ik_1r}}{r}-\frac{e^{ik_1r_2}}{r_2}+\int_{-\infty}^{\infty}\frac{1}{l+\tau^2 m}H_0^{(1)}(\lambda\rho)e^{-(z+a)l}\lambda d\lambda.$$

So, if the vertical dipole is of finite height its Q_2 is (9) with a factor $2/(1+\tau^2)$ added and z replaced by $z+a$.

The Effect of Inductance on the Intermittent Glow Discharge

WINSTON E. KOCK,* *University of Cincinnati*

(Received May 20, 1933)

The insertion of an inductance in the condenser arm of an intermittent glow discharge circuit was found to affect the characteristics of the oscillations. The voltage-frequency curve was noticeably altered, the wave form of the voltage across the condenser became sinusoidal and other new wave forms were introduced. Within a certain range, the frequency of oscillation was practically independent of the voltage, resistance or tube characteristics. Various applications are suggested.

INTRODUCTORY

THE intermittent glow discharge, first noticed by Gassoit[1] and later discussed by Hittdorf,[2] is obtained by placing a condenser in parallel with a discharge tube and a resistance in series with it and a voltage supply (Fig. 1). The approximate wave form of the voltage across the condenser is shown in Fig. 2.[3] The frequency of intermittence is approximately given by[4]

$$f=(RC\log_e(V-V_0)/(V-V_1))^{-1},$$

where V is the applied potential, V_0 is the ignition potential and V_1 the extinction potential of the discharge tube.

The inclusion of an inductance in the condenser arm has been tried by several workers in this field but the effects with which this report is concerned were not recorded.

Herweg[5] first inserted the inductance to check the predictions of Kaufmann[6] regarding the stability of the discharge. He utilized the circuit shown in Fig. 3 and, starting with a low value of R, he gradually increased this resistance until oscillations were produced. Over a very small range of R he obtained oscillations of the first kind, i.e., oscillations wherein the current through the discharge tube never ceased completely; and as R was further increased, he obtained intermittence oscillations of the second kind, oscillations wherein the current through the discharge tube was truly intermittent.

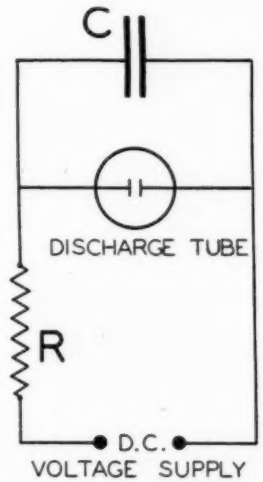

FIG. 1. Circuit diagram for the intermittent glow discharge.

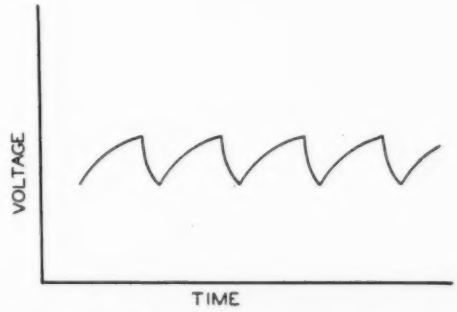

FIG. 2. Wave form of the voltage across the condenser in the intermittent glow discharge.

* Special Fellow in the Department of Physics, University of Cincinnati.

[1] Gassoit, Proc. Roy. Soc. (London) **A12**, 329 (1862).

[2] Hittdorf, Ann. d. Physik **7**, 566 ff. (1879).

[3] Oschwald and Tarrant, Proc. London Phys. Soc. **36**, 262 (1924).

[4] See Pearson and Anson, Proc. London Phys. Soc. **34**, 204 (1922); also R. Anthouard, Comptes Rendus **185**, 188 (1927).

[5] Herweg, Phys. Zeits. **13**, 633 (1912).

[6] Kaufmann, Ann. d. Physik **307**, 175 (1900).

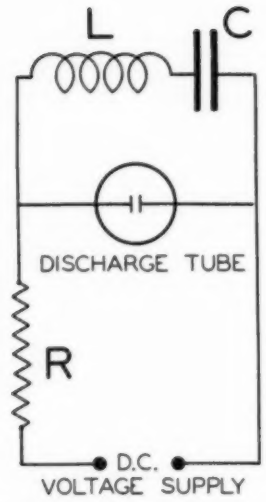

FIG. 3. Circuit diagram of the inductive glow discharge oscillator.

Dallenbach[7] later pointed out that Kaufmann's formula was not applicable to Herweg's circuit unless certain assumptions were made. In 1924, Oschwald and Tarrant[3] noticed that at high frequencies of intermittence, the inclusion of an inductance in the condenser arm had the effect of maintaining oscillations above the limiting frequency otherwise obtainable. Clarkson[8] reported that inductance in the condenser arm facilitated the production of a series of flashes of decreasing intensity. However, no mention has been made of the effect of inductance on the frequency-voltage curves or on the wave forms of the various voltages throughout the circuit; these effects will now be discussed.

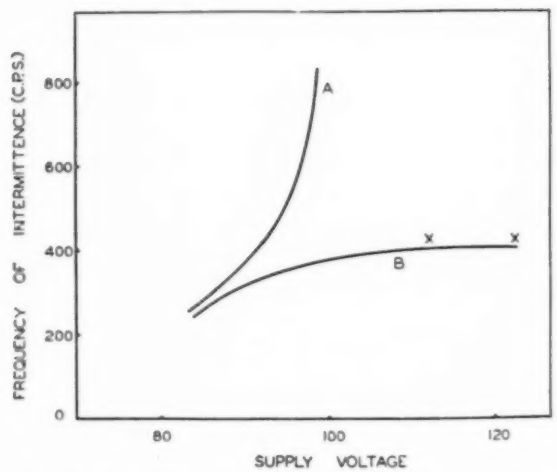

FIG. 4. Frequency-voltage curves; A, the intermittent glow discharge (no inductance, circuit of Fig. 1, $C=0.001$ mf, $R=1$ megohm); B, the inductive glow discharge oscillator (circuit of Fig. 3, $L=150$ henries, $C=0.001$ mf, $R=1$ megohm).

[7] Dallenbach, Phys. Zeits. **27**, 101 (1926).
[8] Clarkson, Phil. Mag. **4**, 849 (1927).

EXPERIMENTAL

In this investigation the inductances were of the order of several hundred henries; for this purpose, the secondaries of small radio transformers (audiofrequency) were admirably suited. Commercial cold-cathode one-watt neon glow lamps were used for the glow discharge tube and batteries were employed for the voltage supply when rectified alternating current was not suitable. Measurements of frequency were made with a Western Electric oscillator and checked with tuning forks; wave forms were observed on a cathode-ray oscillograph and recorded on a Duddell oscillograph.

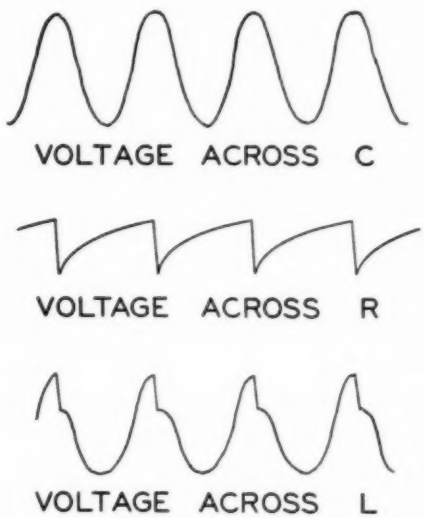

FIG. 5. Wave forms of the inductive glow discharge oscillator when operated in the region $X-X$, Fig. 4.

Frequency-voltage curves are shown in Fig. 4. These curves apply to the circuit of Fig. 3; curve A portrays the characteristic with the inductance short-circuited, whereas curve B shows the characteristic with the inductance operative. For curve B the limiting frequency of intermittence is that frequency at which the oscillating circuit

resonates and corresponds to the frequency of Herweg's[5] oscillations of the first kind, i.e., $f=1/2\pi(L'C')^{\frac{1}{2}}$, where C' includes the inter-electrode capacity of the tube and L' includes the effective inductance of the tube. The frequency is seen to be practically independent of the voltage over a large region (portion X–X); if the frequency is plotted against values of the series resistance, the same flat characteristic is obtained. It is also evident that ordinary changes in the tube constants will not appreciably affect L' and C', hence, for the region X–X, the frequency is little affected by variations in voltage, resistance or tube constants.

Various wave forms are shown in Fig. 5. Comparison with Fig. 2 indicates the change which the voltage across the condenser undergoes when the inductance is inserted. The new wave is very nearly sinusoidal if the tube is operated in the region X–X, Fig. 4. However, the voltage across the series resistance is not greatly affected, because of the absence of inductance effects in the outer branch circuit.

Suggested Applications

For a.c. bridge measurements and other experiments where harmonics in the voltage wave are objectionable, the inductive glow discharge oscillator offers a convenient and simple sine wave generator of practically constant frequency. Inasmuch as the voltage swing on the condenser is of the order of five to ten volts, only one stage of amplification would be required to provide a fair power output. Variations in frequency can be introduced by a variable condenser, thus affording a sine wave oscillator of large frequency range.

The inductive glow discharge oscillator is being utilized by the author for the electrical production of music. The remarkable pitch stability over the region X–X, Fig. 4, makes this circuit an excellent source of vibrations for an electro-musical instrument, wherein a separate discharge tube is employed for each note of the scale. A description of this instrument will appear in a later article.

The Temperature Distribution of a Gas Flowing Through a Furnace

K. F. HERZFELD, *The Johns Hopkins University, Baltimore, Maryland*

(Received July 27, 1933)

In recent experiments the heat of chemical activation (formation of radicals) has been determined by measuring temperature coefficients of reaction rates of gases flowing through a furnace. To justify this procedure, an investigation is necessary to find out to what extent temperature equilibrium is reached. In this paper it is shown that the flow is laminar, and that two cases must be distinguished. Temperature equilibrium is reached throughout the flow when the pressure drop is less than 0.003 mm Hg per cm. For pressure drops about ten times as high, only a thin sheet close to the wall reaches temperature equilibrium, but this fact affects only the total number of activated molecules reaching the wall, not the temperature coefficients.

IN recent experiments, the behavior of gases flowing through a cylindrical furnace at low pressure and high speed has been studied. The number of radicals produced in the furnace has been used as a basis on which to calculate the heat of activation. It is, of course, of primary importance to determine whether temperature equilibrium has really been attained.

A. The Flow

The flow in this case is given by Poiseuille's formula[1]

$$p_1-p_2=u_m(4\eta L/r_0^2)+0.54\rho u_m^2, \qquad (1)$$

where p_1-p_2 is the pressure difference over the tube length L, r_0 the radius of the tube, ρ and η density and viscosity of the gas, u_m the maximum velocity in the center; at other places we have

$$u=u_m(1-r^2/r_0^2), \qquad (2)$$

with the average

$$\bar{u}=u_m/2. \qquad (2')$$

In a case such as the one treated by Rice,[2] where $p_1-p_2=0.5$ mm $=660$ dynes/cm^2, $L=30$ cm, $r_0=0.5$ cm, $\rho=0.85\times10^{-6}$ (ethane, 0°C), $\eta\sim10^{-4}$, one finds

$$u_m\sim1.2\times10^4 \text{ cm/sec.} \qquad (3)$$

Even then, however, the flow is not turbulent, because the Reynolds[3] number is only

$$R=\bar{u}r_0\rho/\eta=50 \qquad (3')$$

(due to the small density) while the limit for turbulent flow is above 1000.

In another case,[4] where the pressure drop is 0.003 mm per cm, $u_m=2500$ cm/sec., $R=6.3$ (pressure 0.3 mm).

B. Heat Conduction; General Equation and Slow Flow

The equation of heat conduction is (λ heat conductivity, C' specific heat per cc).

$$\frac{\lambda}{C'}\left(\frac{\partial^2T}{\partial r^2}+\frac{1}{r}\frac{\partial T}{\partial r}+\frac{\partial^2T}{\partial x^2}\right)-u\frac{\partial T}{\partial x}=0. \qquad (4)$$

This equation has been integrated if u is independent of r.[5]

We can write $\lambda=\alpha C'\eta/\rho$ where α is of the order of magnitude 1 (2.5 for a monatomic gas).

The solution given in the reference above, however, is useful only if

$$\beta=u_0r_0C'/2\lambda=u_0r_0\rho/2\alpha\eta=R/2\alpha \qquad (5)$$

is not large compared with 2.4. This condition is not fulfilled by the conditions of the experiment

[1] Handb. d. Exper. Physik, Vol. IV-4, pp. 41, 46, Leipzig, 1932.

[2] F. O. Rice and Sister M. Denise Dooley, J. Am. Chem. Soc. 55, Oct. (1933).

[3] Reference 1, p. 9.

[4] W. R. Johnston, Diss., Johns Hopkins Univ. (1933).

[5] F. Paneth and K. F. Herzfeld, Zeits. f. Elektrochemie **37**, 577 (1931).

of Rice and Dooley, but is fulfilled in the case of Rice and Johnston.[4] Here $\beta = 6.3/5 \sim 1.3$ and the expression

$$\beta - (\beta^2 + 2.4^2)^{\frac{1}{2}} = -1. \qquad (6)$$

The temperature difference falls off according to

$$e^{-x/r_0} \sim 10^{-x/1.15}.$$

This means that the gas has reached the wall temperature within 1 percent throughout while traversing a distance less than 3.5 cm. If $R/2\alpha$ is small compared with 2.4, then a distance of only $l = 2r_0$ would be required to reach temperature equilibrium up to 1 percent (this error would also affect the temperature coefficient to 1 percent only).

C. Heat Conduction; Rapid Flow

Here, however, with $R = 50$, the velocity is far too high to attain equilibrium over the whole cross section. Accordingly it is essential to take into account the fact that according to (2) the gas moves more slowly near the walls than in the body of the gas. We shall find in the following that there is a thin layer near the wall which closely attains temperature equilibrium, while the temperature of the core of the gas stream does not rise very high. In Rice's experiment the test mirror is only a short distance (1 to 2 cm) beyond the end of the furnace. We shall attempt to give an approximate description of the mechanism according to the subsequent calculations: Close to the walls there will be a thin sheet of gas in which the number of radicals corresponds to the temperature of the wall; the core will be relatively cold and will have only a negligible number of radicals. Because of the form of Arrhenius' equation, with the rapid decrease of activated particles with falling temperature, only the *highest* temperature counts. At the mirror then, there will be a diffusion of molecules and radicals from the hot "layer" and of molecules from the "cold" core. The latter act only as dilutants, and the amount of dilution is nearly independent of the temperature of the furnace. Accordingly, the temperature coefficient of the number of radicals is very little affected by the fact that they come from only a small fraction of the gas, though the absolute number (which does not interest us here) is, of course, greatly diminished.

The calculation is made in the following manner.[6] If heat conduction proceeds only in a thin sheet of gas adjacent to the walls, the curvature of this sheet can be neglected; that is, the problem can be treated as the heat conduction by flow along a plate. This case has been calculated approximately by Pohlhausen.[7]

Let y be the distance from the wall $(= r_0 - r)$. Then his Fig. 2 (reference 7, p. 120) shows that (when T_1 = temperature of wall, T_0 = original temperature of gas, and L' = length of furnace)

$$\frac{T - T_1}{T_1 - T_0} = -0.3\left(\frac{u_m \rho}{\eta L'}\right)^{\frac{1}{3}} y = -0.3\left(\frac{2R}{r_0 L'}\right)^{\frac{1}{3}} y \qquad (7)$$

(at about 1 mm distance, $(T - T_1)/(T_1 - T_0) \sim 8$ percent according to his figure).

If the number of radicals in 1 cc at temperature T_1 is given by

$$N_1 = N' e^{-E/\mathbf{R}T_1} \qquad (8)$$

we find at the distance y

$$N = N' e^{-E/\mathbf{R}T} = N' e^{-E/\mathbf{R}T_1} e^{-Cy} = N_1 e^{-Cy} \qquad (9)$$

where

$$C = 0.3 \frac{E}{\mathbf{R}T_1} \frac{T_1 - T_0}{T_1} \left(\frac{2R}{r_0 L'}\right)^{\frac{1}{3}}. \qquad (10)$$

D. The Diffusion Problem

We will consider next the problem of the diffusion of the radicals to the wall after leaving the furnace. Again, the equation of diffusion is given by (D = coefficient of diffusion)

$$D\left(\frac{\partial^2 N}{\partial r^2} + \frac{1}{r}\frac{\partial N}{\partial r} + \frac{\partial^2 N}{\partial x^2}\right) - u\frac{\partial N}{\partial x} = 0. \qquad (11)$$

We can simplify this equation by considering the important sheet as a plane (neglecting $(1/r)(\partial N/\partial r)$); furthermore, we can neglect the effect of lengthwise diffusion ($D\partial^2 N/\partial x^2$) as compared with that of convection ($u\partial N/\partial x$), so that (11) takes the form

$$D\,\partial^2 N/\partial y^2 = u\,\partial N/\partial x. \qquad (11')$$

[6] It has not been possible to integrate (4) suitably, taking account of (2).

[7] E. Pohlhausen, Zeits. f. angew. Math. u. Mech. **1**, 115 (1921).

In integrating this equation, we will neglect the variation of u near the wall, that is put $u=\bar{u}$, which means a *decrease* of diffusion to the wall. Then (11′) has the familiar form of the equation of one dimensional heat conduction with N_0 instead of T, and x instead of t. Introducing the abbreviation

$$\bar{u}/4Dx=j,$$

where x is the distance of the mirror from the furnace, the solution becomes

$$N=N_0(j/\pi)^{\frac{1}{2}}e^{-iy^2}. \qquad (12)$$

This, however, would be the distribution of N_0 radicals starting from $y=0$, $x=0$. As the initial distribution at $x=0$ (end of the furnace) is given by (9), we find ultimately that

$$N=N_1(j/\pi)^{\frac{1}{2}}\int_0^\infty e^{-Cy'}e^{-i(y-y')^2}dy'. \qquad (13)$$

The number of radicals reaching a cm² of the wall per second through diffusion is

$$Z=+D(\partial N/\partial y)_{y=0}$$

or

$$Z=2N_1D(j^3/\pi)^{\frac{1}{2}}\int_0^\infty e^{-Cy'-iy'^2}y'dy'. \qquad (14)$$

This can be transformed into

$$Z=2N_1D(j/\pi)^{\frac{1}{2}}\left\{\tfrac{1}{2}-\frac{Ce^{C^2/4j}}{2j^{\frac{1}{2}}}\int_{C/2j^{\frac{1}{2}}}^\infty e^{-\omega^2}d\omega\right\}. \qquad (14')$$

The numerical value of this expression depends on

$$\frac{C^2}{4j}=0.18\left(\frac{E}{\mathbf{R}T_1}\frac{T_1-T_0}{T_1}\right)^2\frac{R}{r_0L}\frac{Dx}{\bar{u}}$$

$$=0.18\left(\frac{E}{\mathbf{R}T_1}\frac{T_1-T_0}{T_1}\right)^2\frac{x}{L}\frac{\rho D}{\eta}. \qquad (15)$$

But the theory of gases in its corrected form gives for the diffusion of an impurity (radical) present in small quantities[8]

$$D\rho/\eta=3b^2/5 \qquad (15')$$

where b is a numerical coefficient of order one defined by

$$b^2=(1+M/M')^{\frac{1}{2}}1/[1+(d'/d)^2]$$

(d is the radius of collision; the primed quantities refer to the radical, the unprimed to the molecule).

Therefore, introducing the abbreviation W, $(W=C/2j^{\frac{1}{2}})$ (15) becomes

$$W=0.33\frac{E}{\mathbf{R}T_1}\frac{T_1-T_0}{T_1}b\left(\frac{x}{L'}\right)^{\frac{1}{2}}. \qquad (15'')$$

This has a value of approximately 2 in the case in which we are interested. With any value larger than 1, we have[9] for

$$\tfrac{1}{2}-We^{W^2}\int_W^\infty e^{-\omega^2}d\omega=\frac{1}{4W^2}\left(1-\frac{3}{2W^2}+\frac{15}{4W^4}\cdots\right), \qquad (16)$$

$$Z=N_1\left(\frac{\bar{u}D}{r_0x}\right)^{\frac{1}{2}}\frac{1}{4W^2}\left(1-\frac{3}{2W^2}+\frac{15}{4W^2}\cdots\right). \qquad (17)$$

The temperature coefficient of (17) is practically that of N_1 (see (8)), as the factor $(1/W^2)(1-3/2W^2+15/4W^2)$ changes approximately as $T^{-2.5}$. The limits for our formula are:

$R\ll 1000$ laminar flow, Eq. (3′)

$2Rr_0/L'\gg 1$ to give a thin hot sheet, (7)

$W\geqq 2.$ (15″)

Two more remarks must be made: We have treated only the heat transfer to translational and rotational degrees of freedom, which are measured by λ, but not the vibrational, which are really responsible for the breaking of the bond. Now if, as is probable, this latter transfer is slow[10] that does not alter our calculations, so long as its temperature coefficient is small (or entirely absent). For example, if it took a number N'' of collisions with sufficient energy for the

[8] D. Enskog, Phys. Zeits. **12**, 56, 533 (1911); Ark. f. Math. Astr. och. Fys. **16**, No. 16 (1922).

[9] E. Jahnke and P. Emde, Funktionentafeln, Leipzig, p. 31, 1909.

[10] If the heat transfer to vibrational degrees of freedom should be about as fast as the one to translational degrees, it would not affect the calculation for the rapid flow while it would increase the necessary length of the furnace in the slow flow somewhat.

excitation of the vibrations, this would diminish the absolute number but would not change the temperature coefficient. Secondly, in our calculations we have neglected the fact that due to the change of temperature η and ρ change in the furnace. This will again not modify the temperature coefficient sufficiently to be of any significance.

Of course, the velocities u are so high (close to sound velocity), that the use of the Poiseuille formula might be debatable, but nothing better is available.

Ionization Time of Thyratrons

L. B. SNODDY, *General Electric Research Laboratory*

(Received June 27, 1933)

The ionization time for four types of commercial Thyratron tubes has been determined for the following cases: (1) impulsive voltage applied to the anode with the grid biased positively or negatively, (2) impulsive voltage applied to the grid with the anode potential constant, and (3) impulsive voltage applied to grid and anode simultaneously. The principal factors in fixing the ionization time are (1) the tube design; (2) the mercury vapor pressure (the time lag in starting is increased and made more erratic by decreasing the vapor pressure); (3) the grid bias (increasing the bias negatively increases the time lag); (4) the steepness of the wave front applied to the system. The lags become less as the rate of building up of voltage increases. This is due partly to the higher voltages reached and partly to the greater induced grid voltages when the impulse is applied to the anode. This effect is computed for two kinds of applied voltage waves. The time between grid and anode breakdowns was measured for an FG-41 and an FG-17. The grid and anode currents during this interval were computed. For the particular FG-41 used, $i_{\text{anode}}=3i_{\text{grid}}$. A table of ionization times under these various conditions is given for four Thyratron tubes (FG-17, 33, 41, 57).

IN all gaseous discharge devices initially in an unconducting state there is a definite time lag between the application of potential to the device and the attainment of maximum conduction. During this time the gas path is ionized and the necessary emission built up at the cathode. In tubes containing emitting cathodes, such as the Thyratron tube, this delay allows the production and movement of positive ions to take place in sufficient numbers to neutralize the negative space charge at the cathode. A measurement of this lag in various types of Thyratron tubes was made some time ago and a brief report published.[1] In view of the increasing use of Thyratron tubes in scientific investigations it was thought worth while to give the detailed results.

The time lag of Thyratron tubes has also been measured by Nottingham[2] and by Koch.[3] The method used by Nottingham did not allow the actual delays to be measured, as intervals shorter than about 20×10^{-6} sec. could not be measured accurately. However he was able to determine that the actual lags were probably considerably less than this amount. The results of Koch are very accurate and of high time-resolving power. He obtained time lags ranging from about 1.5×10^{-7} sec. up to a number of microseconds (10 to 20), the exact value depending upon the experimental conditions. However, they refer to specia! tubes and the method of applying the potential is not that ordinarily used with the Thyratron tube. In his work an impulsive potential was applied to the anode with the grid biased by different amounts from a constant voltage source. In the usual Thyratron tube circuits it is customary to apply the impulse to the grid with the anode kept at constant potential. The lag in the two cases may be quite different. Both of these methods were used in the present work.

The impulsive potential was applied by a condenser circuit with a spark gap as the connecting switch and the lags were determined by a cathode-ray oscillograph of the high voltage Dufour type (G.E. HC-2).

The circuit shown in Fig. 1 was used for the determinations in which a positive potential was applied to the anode. The condenser C_1 was used as the source of potential. In all this work it was

[1] A. W. Hull and L. B. Snoddy, Phys. Rev. **37**, 1691A (1931).

[2] W. Nottingham, J. Frank. Inst. **211**, 751 (1931). The long apparent time lags (of the order of 1000×10^{-6} sec.) observed by Nottingham in his first paper on Thyratrons (J. Frank. Inst. **211**, 271 (1931)) were due to an incorrect method of measurement.

[3] W. Koch, Phys. Zeits. **33**, 934 (1932).

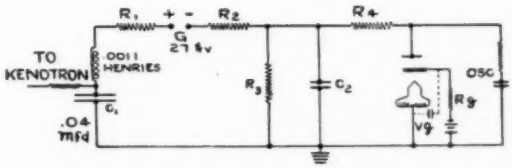

FIG. 1. Circuit used to apply an impulsive potential to the anode of the Thyratron with the grid biased by the battery V_g through the resistance R.

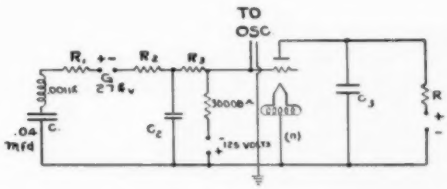

FIG. 3. Circuit for applying an impulse to the grid with the anode at constant potential.

charged to 27 kv. The wave front was varied by changing R_1, R_2, R_3 and C_2. The rate of discharge through the tube after breakdown was limited by R_4. The grid was biased by the battery V_g through the resistance R_g.

An oscillogram, typical of this arrangement, is given in Fig. 2. The kind of voltage wave

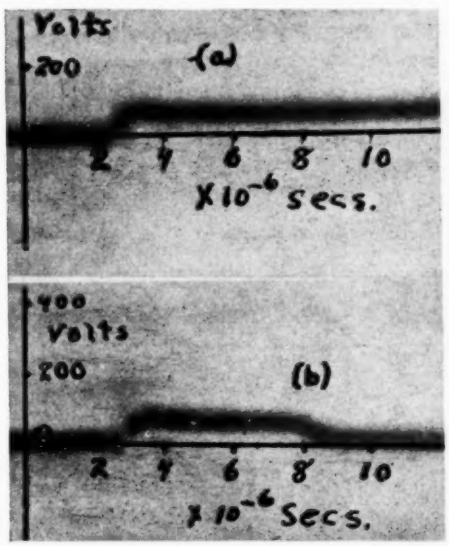

FIG. 2. Oscillogram showing the type of breakdown obtained with the circuit of Fig. 1. The applied voltage wave is shown at a and breakdown on this wave at b. Thyratron FG-17 with $V_g = -6.9$ volts and $R_g = 1000$ ohms. Condensed mercury temperature of 35°C.

applied to the tube is shown at a, and the breakdown on this wave at b. The tube used was an FG-17 with $V_g = -6.9$ volts and $R_g = 1000$ ohms.

The circuit used to apply the impulsive potential to the grid with the anode at constant voltage is shown in Fig. 3. The grid was usually kept at -125 volts before the start of the impulse. With the oscillograph connected as shown, the time lag in grid breakdown could be determined but no indication of the anode breakdown would be obtained. Fig. 4a is an oscillogram typical of this method. The grid discharge starts at t_1 and is complete at t_2. The tube is an FG-41 with an anode potential of 125 volts.

The total time of breakdown was measured by introducing a resistance of 1000 ohms at r. The current through this resistance raises the potential of the cathode and consequently that of the grid. In this way the two stages in the dis-

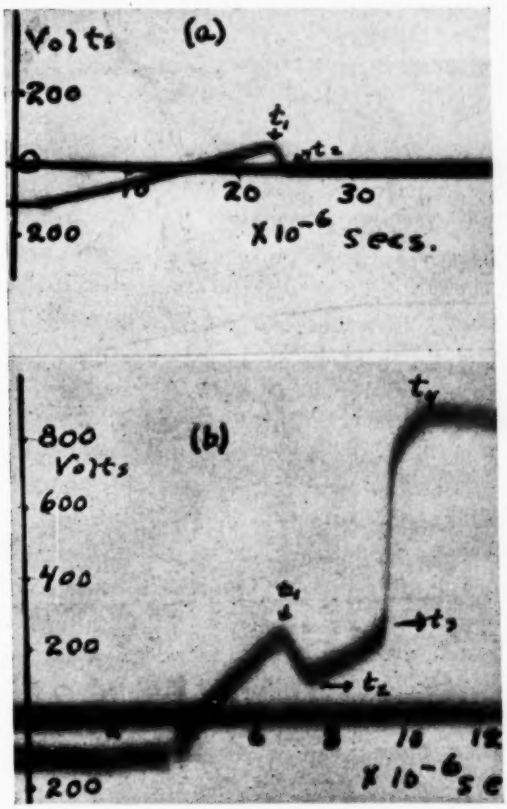

FIG. 4. a. Starting of grid discharge with the circuit at Fig. 3. The breakdown starts at t_1 and is complete at t_2. Grid initially at -125 volts. Anode potential $+125$ volts. b. Grid voltage after addition of 1000 ohms at r. Grid discharge complete at t_2—anode breakdown at t_3. FG-41 with mercury temperature at 40°C.

charge can be distinguished. This is illustrated in Fig. 4b. The grid discharge starts at t_1 and is complete at t_2; the anode breakdown occurs at t_3. An FG-41 was used for this picture with an anode potential of 870 volts and a mercury temperature of 40°C. The grid voltage rose to 220 volts before breakdown. The total time of breakdown is 4.9×10^{-6} sec.

This method was checked with the arrangement of Fig. 5. The spark gap G is coupled to the deflection plate circuit of the oscillograph

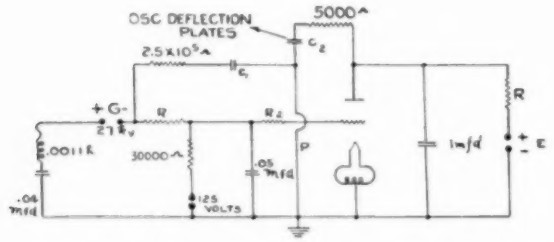

FIG. 5. Circuit arranged to determine total time lag when impulse is applied to grid. Arc over of G registered on oscillograph plates by means of the small coupling capacity C_1.

by the capacity C_1 (about $20\mu\mu$f) and a 2.5×10^5 ohm resistance, as shown. Because of the inductance of the connecting wire P, sufficient voltage appears across the deflection plates to register the breakdown of G. With the wave front applied to the grid known, the total time lag can easily be determined.

This is shown in Fig. 6 for an FG-41 with a constant applied anode potential of 125 volts and a mercury temperature of 35°C. The breakdown of G is registered at t_1; the discharge of the Thyratron tube starts at t_2 and is completed at t_3. The interval t_2-t_1 is made up of two parts: (1) the time required to change the potential of the grid and its parallel 0.05μf capacity from -125 volts to the breakdown grid potential; and (2) the time between grid and anode breakdowns. With the breakdown potential of the grid known for this particular wave the time between grid and anode discharge can be determined.

The results of the tests are summarized in Table I. The voltages given are in every case the maximum values. In some of the work the grid and anode were connected together and the

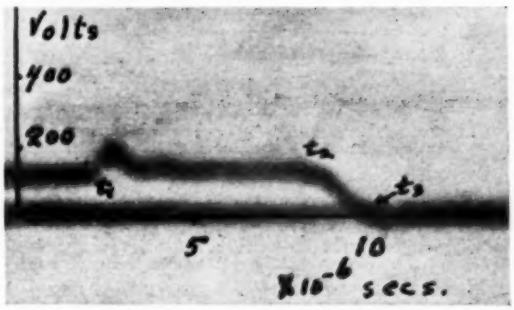

FIG. 6. Oscillogram of anode potential when using circuit of Fig. 5. Arc over of G at t_1. Discharge starts at t_2 and is completed at t_3. FG-41 with mercury temperature of 35°C.

breakdown time determined for the combination. This is indicated in the table by equal grid and plate voltages. A grid bias and resistance (V_g and R_g) were used only in the cases in which an impulsive potential was applied to the anode. The negative values of V_g represent the minimum grid potential at which consistent starting could be obtained with the given voltage impulses.

By a study of the table the most important factor in determining the time lag for any particular tube is seen to be the mercury vapor pressure. A decrease in pressure not only lengthens the starting time but also causes it to become more erratic.

A negative bias also increases the lag as would be expected. On the other hand, the delay with a positive bias does not appear to be very sensitive to changes of several volts in the value of V_g. With very steep waves the value of V_g seems to have very little to do with the lag, provided it is not negative enough to prevent starting. The reason for this is probably to be found in the finite inter-electrode capacities of the tubes.

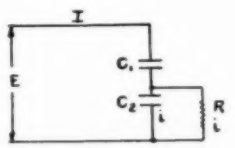

FIG. 7. Equivalent tube circuit.

In Fig. 7 the equivalent tube circuit for an impulse applied to the anode is drawn with C_1 representing the anode-grid capacity, C_2 the grid-cathode capacity and R the grid resistance.

TABLE I. *Summary of tests on time lag of Thyratron tubes.*

Tube code No.	Hg pressure microns	V_g (volts)	R_g (ohms)	Grid voltage maximum	Anode voltage maximum	Time lag grid (10^{-6} sec.)	Time lag grid to plate breakdown (10^{-6} sec.)	Total time lag (10^{-6} sec.)	Remarks
FG-17	6	+9.3	1000		462←→396			3.3←→2.8	Linear wave. $\Delta V/\Delta t = 1.65\times10^8$ volts/sec.
	6	+9.3	1000		924←→550			1.2←→0.7	$\Delta V/\Delta t = 1.85\times10^9$ volts/sec.
	15.5	+6.2	1000		176←→110			1.3←→1.0	1.65×10^8 volts/sec.
	4.1	+5.3	1000		77			4.0	Flat wave
	4.1	+2.4	1000		77			3.25	max.
	4.1	−6.9	1000		77			4.2←→6.9	in 6.7×10^{-7} sec.
	8.8			44	264	—	0.95	0.95	Fig. 3. $r = 1000\Omega$
	8.8			66	66			0.83←→0.95	Grid and anode connected
FG-33	20.5	+6.25	1000		99			1.5	Flat wave
	20.5	+3.13	1000		99			1.8	" "
	20.5	−1.6	1000		99			3.2	" "
	20.5			88	88			1.1	Grid and plate connected
	4.1	+6.3	1000		99			6.4	Flat wave
FG-57	20.5	−3.15	1000		99			3.1←→2.7	Flat wave
	20.5			88	88			1.3	" "
	4.1			99	99			12←→5.8	" "
FG-41	6			220	858(const.)	2.1	2.8←→3	4.9←→5.1	Fig. 3. $r = 1000\Omega$
	6			220	462	2.1	3.4	5.5	Fig. 11
	6			176	125(const.)	(3.2)		5	Fig. 5
	6			66	66	grid and plate		9.3←→8.6	8×10^6 volts/sec.
	6			154	154	connected		4.5	8×10^7 volts/sec.
	4.1			176	125(const.)	3.2	2.2	5.4	8×10^7 volts/sec.
	4.5			88	125(const.)	3.7	29	32.7	Flat wave

With a voltage $E = kt$ applied to this combination the potential of C_2 is given by

$$V_{C_2} = kRC_1[1 - \exp[-t/(RC_1 + RC_2)]]. \quad (1)$$

This is plotted in Fig. 8 for an FG-17 and an FG-41. The constants used are given below:

Tube	C_1	C_2	R
FG-17	4.7×10^{-12} f	10.0×10^{-12} f	1000 ohms
FG-41	10.4×10^{-12} f	31.3×10^{-12} f	1000 ohms

The two rates of voltage increase given in Table I were used: $k = 1.65\times10^8$ volts/sec. and 1.85×10^9 volts/sec. For an applied voltage of the form $E = E_{max}(1-\epsilon^{-\alpha t})$ the potential of C_2 is given by:

$$V_{C_2} = \frac{E_{max}\alpha RC_1}{1-\alpha[RC_1+RC_2]}[\epsilon^{-\alpha t} - \epsilon^{-t/(RC_1+RC_2)}]. \quad (2)$$

This is shown in Fig. 9 for the same Thyratron tubes and with two values of α: 0.25×10^7 sec.$^{-1}$ and 0.25×10^8 sec.$^{-1}$.

It is obvious that this induced grid voltage may be amply sufficient to start the Thyratron tube provided the grid is not initially negative enough to compensate for this effect. This is much more likely to be effective at high temperatures with the short time lags, especially so in the second case (Fig. 9) where the induced voltage is of relatively short duration.

This difficulty may be overcome by connecting an additional capacity with short lengths of wire between the grid and cathode, as indicated by the dotted lines in Fig. 1. With an added capacity of 0.01μf the rate of increase of V_{C_2} for condition d of Fig. 8 is changed to that shown at e. The change in grid voltage is reduced to a negligible amount by this addition. For a potential wave of the form $E = E_{max}(1-\epsilon^{-\alpha t})$ the effect would be even more pronounced.

It is evident that increasing the resistance in the grid circuit would raise the induced grid voltage with this type of impulsive starting (impulse applied to anode) and so decrease the

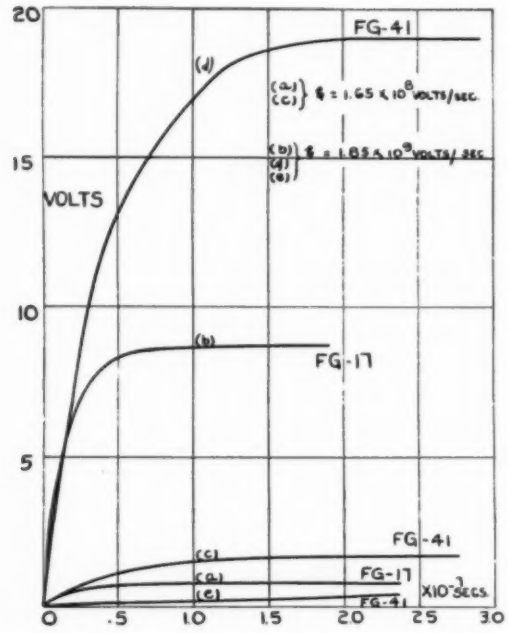

FIG. 8. Graph of induced grid voltage with $E=kt$ applied to anode. e. 0.01 μf added capacity between grid and cathode. Otherwise same as d.

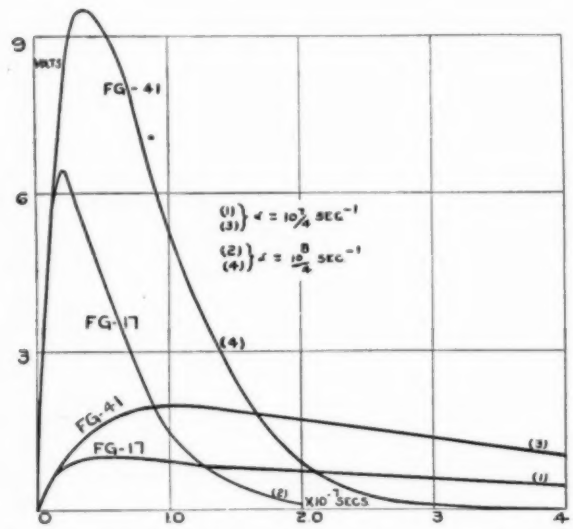

FIG. 9. Induced grid voltage with $E=E_{max}(1-\epsilon^{-\alpha t})$ applied to anode. $E_{max}=100$ volts.

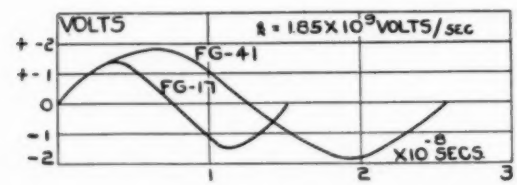

FIG. 10. Induced grid voltage with $E=kt$ and R of Fig. 7 replaced by an inductance $L=4\times10^{-7}$ henries.

lag at high temperatures. This agrees with the work of Koch who obtained decreasing lags as he increased the grid resistance.

When R of Fig. 7 is replaced by an inductance L, the grid voltage, for $E=kt$, is given by:

$$V_{c_2}=kC_1(L/(C_1+C_2))^{\frac{1}{2}}\sin(t/(LC_1+LC_2)^{\frac{1}{2}}). \quad (3)$$

This is plotted in Fig. 10 for an FG-17 and for an FG-41 with $k=1.85\times10^9$ volts/sec. and $L=4\times10^{-7}$ henries. From this it is seen that the inductance of any ordinary loop of connecting wire in the grid system would not have an appreciable effect upon the starting time wave fronts of this steepness.

The current flowing in the grid and anode circuits between the times of grid and anode breakdowns (t_2-t_3 of Fig. 4b) can be computed from the circuit constants and the grid voltage measured on the oscillogram. The constants used for Fig. 4b are as follows:

$R_1=34{,}000$ ohms	$C_3=0.05\mu$f
$R_2=14{,}000$ ohms	$R=10^6$ ohms
$R_3=5000$ ohms	$r=1000$ ohms
$C_2=0.004\mu$f	$E=870$ volts

Since the time constant RC_3 is large, the influence of E may be neglected during the interval t_3-t_2. The existence of a definite current to the anode during the time t_3-t_2 was established by changing C_3 from 0.05μf to 0.0008μf. An oscillogram with this value is given in Fig. 11. Although C_3 was charged in both cases to the same voltage (870 volts), the maximum appearing at t_4 in Fig. 11 is only 462 volts, while in Fig. 4b it is 858 volts. The latter agrees within the experimental error with E. The decrease in voltage for the case of Fig. 11 is evidently caused by the anode current flowing during the interval t_3-t_2, discharging the condenser C_3 (R is too high to allow appreciable current from the battery E). The amount of charge lost by C_3 is 3.2×10^{-7} coulombs. This quantity corresponds to a change in potential of only 6 volts when C_3 is 0.05μf, which would not be detected by the oscillograph.

The grid voltage from t_2 to t_3 can be represented by $V_g=a+Kt$, where a and K can be measured from the oscillogram. Assuming that the charging current to C_2 is constant during

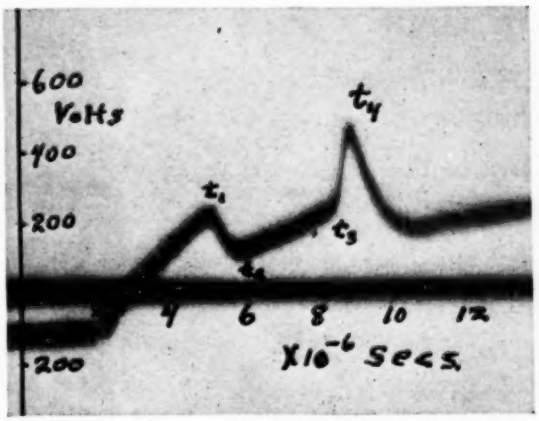

FIG. 11. Oscillogram of grid voltage for circuit of Fig. 3 with $r=1000$ ohms. $C_3=0.0008$ μf.

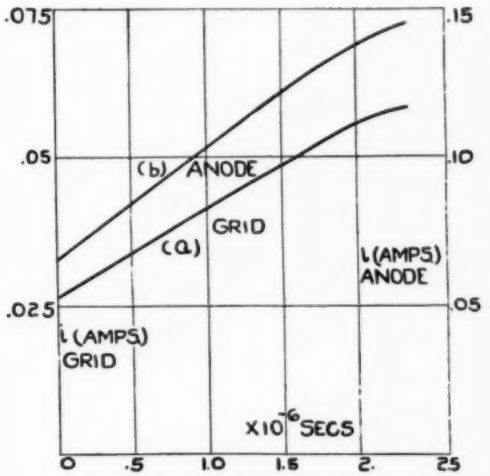

FIG. 12. a. Net current to grid for the interval t_3-t_2 computed from the oscillogram of Fig. 11. b. Anode current during same interval.

this time, the net grid current is easily computed, with the result shown in Fig. 12a.

The anode current may be calculated by two methods: (1), by assuming that the grid voltage measured on the oscillogram is given by V_g (measured) = (20 volt grid-cathode drop) $+i_g \times 1000 + i_{anode} \times 1000$; (2), by assuming that $i_{anode} = A i_{grid}$ where A is a constant of proportionality. Since the total charge transferred is known, the plate current can be obtained from an integration of the grid current time curve. The quotient of 3.2×10^{-7} by the result of this integration gives A. For this particular tube $i_{anode}=3\ i_{grid}$. The results of the two methods are identical within the experimental error involved in reading the oscillogram. The anode current is plotted in Fig. 12b. The actual ratio between the two currents probably depends primarily upon the tube geometry. An FG-17 in the same circuit shows much less net grid current during the interval between grid and anode breakdowns, while the anode current is considerably larger.

The lag between grid and anode breakdowns averages 0.53×10^{-6} sec. less with $C_3=0.05\mu$f than with $C_3=0.0008\mu$f. This decrease is probably due to the constant high plate voltage prevailing in the first case.

The net current to the grid at the point t_1 (Fig. 11) may also be computed. The circuit constants, however, were not measured with sufficient accuracy to allow anything more than an approximate estimate of this current to be made. All that can be said is that it does not exceed 8×10^{-3} amperes, and it may be much less than this.

Ball Lightning

J. C. JENSEN, *Department of Physics, Nebraska Wesleyan University, Lincoln, Nebraska*

(Received July 21, 1933)

The size, appearance and physical properties of ball lightning has been subject to much controversy and but few accurate data are available. Description is given of a series of five photographs showing luminous masses which were of unusual size and which remained visible in changing form for about 3 minutes. Suggestions for further investigations are given.

ONE of the most difficult phenomena in nature to study is that known as ball lightning. It is so rare that comparatively few persons have ever seen it, and these observers have been so startled that they cannot give a clear description of what they saw. Even a trained scientist finds extreme difficulty in making any worth-while tests or measurements on a ball of blue fire as large as two fists which rolls along the floor for three or four seconds and then collapses with a noise resembling a big firecracker, leaving behind nothing more tangible than the odor of ozone. Yet these are the salient points in the descriptions reported recently by Talman,[1] Reynolds,[2] Mathias,[3] Marchant[4] and Craigie.[5]

During the thunderstorm seasons of 1929, 1930 and 1931, the writer was engaged in a study of the electrical field changes caused by lightning discharges with special reference to relation of the direction of branching of the flash to the sign of the field change.[6] This involved photographing a large number of discharges at night, most of them at close range as the storm center approached or came directly overhead. The path of the storm centers was traced by means of a battery of microbarographs.

During the early evening of August 30, 1930, after a sultry day characterized by local thunderstorms in the surrounding territory to the south, a severe storm of the "line-squall" type developed in the west. The wind had been scarcely perceptible from the southeast but changed to the southwest and increased to twenty or thirty miles per hour between 9:35 and 9:45. Rain, accompanied by high northwest winds, began at 9:53. The barograph record shown in Fig. 1 indicates an increase of 0.28 cm (0.11 inch) in pressure in the front of the storm, followed by a

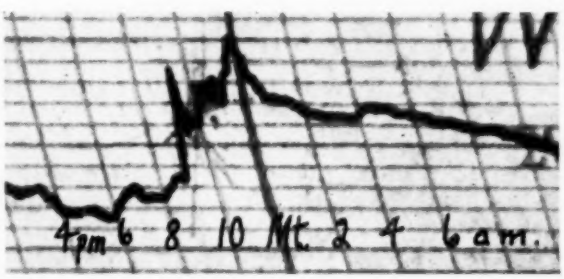

FIG. 1. Microbarograph record, storm of August 30, 1930

second rise of 0.12 cm (0.05 inch) when the active part of the storm, with its rapid convection currents, passed over the instrument. The time on this record is about twenty minutes slow as the first rise began at 9:35.

For making the photographs two cameras were placed in a fourth-story window above the trees and commanding a clear view of the western horizon. One of these is a 5×7 inch Graflex with a Bausch & Lomb Tessar lens rated at f 4.5, the other an Eastman 1A Kodak with f 6.3 lens.

[1] C. F. Talman, Amer. Mercury **26**, 69 (1932).

[2] W. C. Reynolds, Nature **126**, 413 (1930); ibid. **128**, 584 (1931).

[3] E. Mathias, Comptes Rendus **194**, 413 (1932); **194**, 2257 (1933); **196**, 654 (1933).

[4] E. W. Marchant, Nature **126**, 128 (1930).

[5] H. Craigie, Science **42**, 344 (1930).

[6] J. C. Jensen, Monthly Weather Rev. **58**, 115 (1930); Phys. Rev. **40**, 1013 (1932).

2

3

4

5

FIG. 2. First 5×7 inch picture, enlarged.
FIG. 4. Second Graflex picture, enlarged.

FIG. 3. First kodak picture, enlarged. Simultaneous with Fig. 2.
FIG. 5. Third 5×7 inch picture, enlarged.

The cold air rushing ahead of the nimbus cloud was filled with a swirling mass of dust but nevertheless brilliant flashes were seen descending in rapid succession from the cloud to the earth when the first films were exposed at 9:40 P.M. In the wake of one of these flashes which, incidentally, carried negative electricity from cloud to ground, there appeared a shapeless mass of lavender color which seemed to float slowly downwards. The writer was so

occupied with the details of the photographic routine which required the operation of shutters, the use of a stopwatch for timing the lightning-thunder interval, entering data in the notebook, and telephoning to the assistant who had charge of the electrical recording apparatus in the laboratory, that there was little opportunity for close observation of this beautiful but unexpected phenomenon. The rose-colored mass seemed most brilliant near the ground and gave the impression of a gigantic pyrotechnic display. Two or three of the globular structures seemed to roll along a pair of 2300 volt power lines for 100 feet or more, then bounced down on the ground and disappeared with a loud report.

The first five of the fifty films exposed that evening cover an interval of about three minutes and all show the fire-balls in one of their stages. Fig. 2 is an enlargement of the first Graflex picture at 9:40 P.M. The one caught at the same instant with the Kodak, Fig. 3, resembles it closely, the lightning streamers in the rear being identical. Fig. 4 is an enlarged print from the second Graflex negative. It shows the principal descending ball in its most luminous and concentrated form. Although the shutter was open for only a few seconds, two brilliant lightning discharges appear in the background, only one of which is included in the picture. That one, with streamers extending downward, gave a field change which indicated that negative electricity had escaped from the cloud to earth. The Kodak shutter was closed while Fig. 4 was being taken but both cameras caught the final stage as shown in the enlargement of Fig. 5. The Kodak lens was left open longer and shows less detail, together with blurring, due to motion of the illuminated balls.

As mentioned above, some of the fire-balls bounced off a power-line which was about 600 meters (2000 feet) from the observer. From the well-known optical formula relating the size of object and image to object distance and focal length of the lens, the diameter of the first upper ball in Fig. 2 is shown to be 8.5 meters (28 ft) and that in Fig. 4, 12.8 meters (42 ft). Their height above the horizon was 28 meters (92 ft). It will be objected that these dimensions are so much larger than the conventional size that they must relate to different phenomena. However, Toepler[7] states the "masses of light" may vary in size from a hen's egg to 10 meters in diameter. During the course of our researches balls of similar magnitude were seen on another occasion at a distance of two and one-half miles but no photographic record was obtained. In this case also, the balls collapsed with a sharp, loud report.

A tornado which occurred on the evening of July 9, 1932, near Rock Rapids, Iowa, gave evidence of a closely related type of luminous display according to the report of Mr. George Raveling, U. S. Weather Bureau observer. From the sides of the boiling, dust-laden cloud a fiery stream poured out like water through a sieve, breaking into spheres of irregular shape as they descended. No streak lightning of the usual type was observed and no noise attended the fire-balls other than the usual roar of the storm.

While it is not the purpose of this article to propose a scientific explanation for the formation of the phenomenon described above, attention is called to the fact that ball lightning occurs most frequently in connection with dust from a chimney or fire-place, or in the dust-laden air of a wind-squall or a tornado. The interesting laboratory experiments of Cawood and Patterson,[8] in which aerosols 20 cm in diameter and containing many of the characteristics of ball lightning have been produced are suggestive of further work along similar lines. An extension of the theoretical studies of Ollendorff[9] on the pressure, temperature and conductivity relations in the luminous column of a lightning discharge would also be helpful in arriving at a better understanding of the physical factors involved.

---

[7] Max Toepler, Mitteil. d. Hermsdorf Schomburg Isolatoren **25**, 18 (1926).

[8] W. Cawood and H. S. Patterson, Nature **128**, 150 (1931).

[9] F. Ollendorff, Archiv. f. Elektrotechnik **27**, 169 (1933).

Velocity of Elastic Waves in Granite and Norite

L. Don Leet, *Harvard Seismograph Station**

(Received June 17, 1933)

The velocities of elastic waves were investigated in granite at Rockport, Massachusetts, and norite at Sudbury, Ontario. The waves measured were generated by dynamite explosions, and recorded by portable seismographs at distances up to 6260 feet in granite and 10,320 feet in norite. The observed velocities in km/sec. with probable errors indicated by ± were:

	Longitudinal	Transverse	Rayleigh
Rockport granite	5.14±0.005	2.70±0.02	2.19±0.007
Sudbury norite	6.22±0.003	3.49±0.006	2.79±0.01

From these velocities, and the densities of specimens taken from the shooting locations, the following elastic constants may be computed. They are shown below, for comparison, with those computed by a similar procedure in an earlier report for Quincy, Massachusetts, granite.

A quartz-rich zone in the norite was found to transmit the waves with a slower speed. The results are compared with statical measurements of Zisman on rocks from the same locations, a part of the same program of geophysical research at Harvard. Compressibility, measured directly, under hydrostatic pressures, on specimens exposed to the liquid transmitting the pressure is found to be the only statically determined constant which yields seismically effective values. The geological significance of granite velocities and elastic constants is discussed. It is concluded that a longitudinal-wave speed of 5.5 km/sec. cannot be regarded as unique for granite, or even necessarily suggestive of granite, as has been repeatedly proposed; and that there is as yet no seismological justification for the identification of any "layer" of the earth's crust as either sedimentary or granitic.

	Quincy granite	Rockport granite	Average granite	Sudbury norite
Density (grams/cm³)	2.61	2.63	2.62	2.85
Rigidity $\times 10^{-11}$ (dynes/cm²)	1.63	1.92	1.78	3.47
Bulk modulus $\times 10^{-11}$ (dynes/cm²)	4.4	4.4	4.4	6.4
Young's modulus $\times 10^{-11}$ (dynes/cm²)	4.3	5.0	4.65	8.82
Compressibility $\times 10^{13}$ (cm²/dyne)	22.8	22.8	22.8	15.6
Poisson's ratio	0.33	0.31	0.32	0.27

I. Location and Method

In a previous publication[1] some velocities in granite were reported. These included longitudinal waves in Rockport, Massachusetts, granite. The present results represent an extension of that work at Rockport, together with a new investigation of the velocities in the norite of Sudbury, Ontario. Maps of the areas are shown in Fig. 3. The observing stations and shot locations shown there were mapped by plane table, at Rockport on a scale of 300 feet to the inch, and at Sudbury, 400 feet to the inch.

The usual methods of seismic surveying were employed. The elastic waves were produced by the explosion of charges of dynamite. Their arrival at a point at any desired distance from the explosion was recorded by a seismograph placed at that point. The distance travelled by the waves and the time required constituted the observed data. Distances were scaled from the originals of the maps reproduced in Fig. 3.

II. Instruments

The seismographs used at Rockport have been described.[1] At Sudbury, electromechanical-transducer seismographs, known commercially as geophones, were used. They, together with the necessary oscillographs, as well as radios for communication, were the generous gift of Dr. E. L. DeGolyer of the Geophysical Research Corporation. Vacuum-tube amplifiers were interposed between geophones and oscillographs.

* Paper No. 7, published under the auspices of the Committee on Geophysical Research and of the Division of Geological Sciences of Harvard University.

[1] L. D. Leet and W. M. Ewing, Physics **2**. 160 (1932).

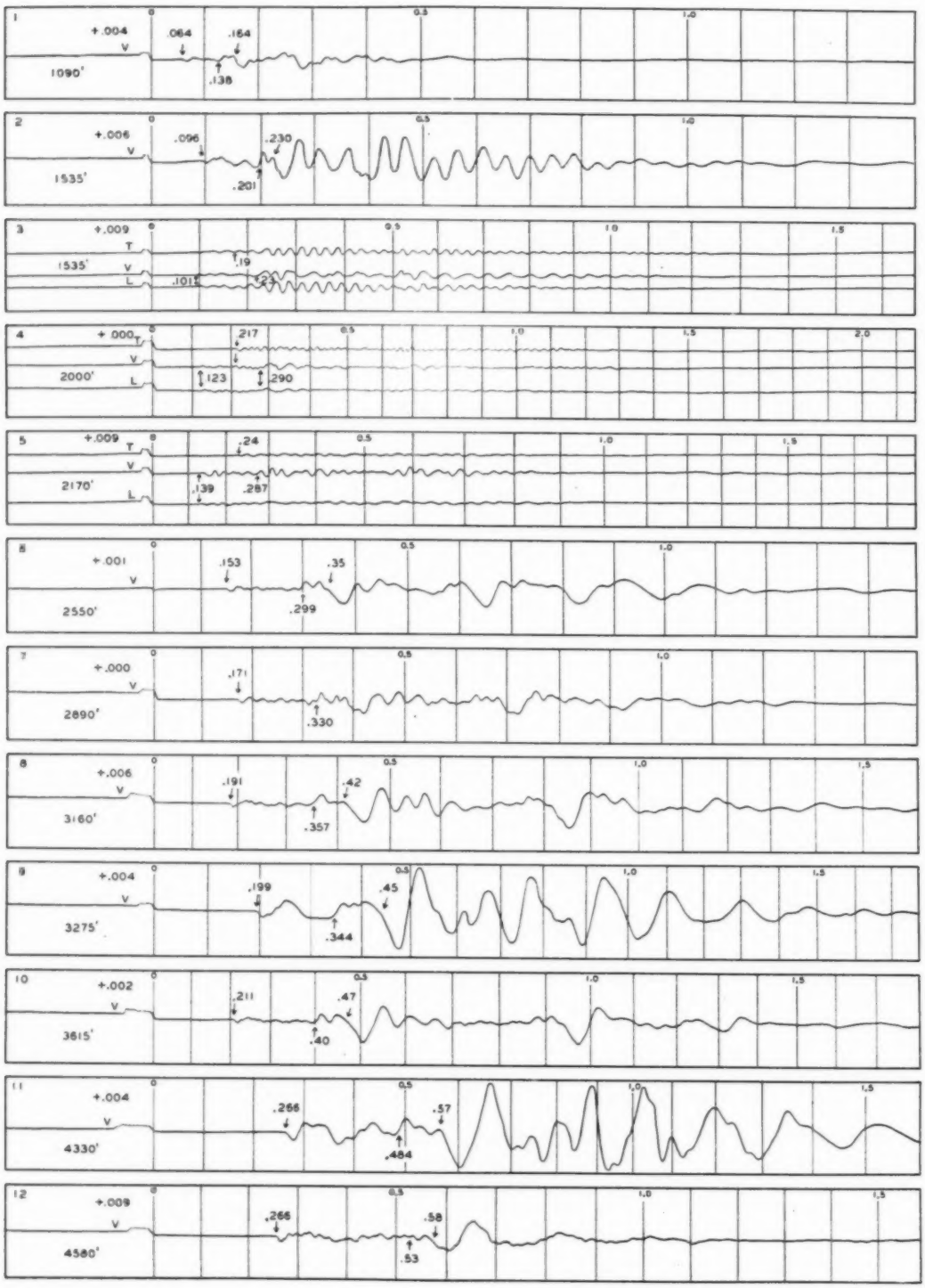

FIG. 1. Specimens of Rockport records.

The explosion of the dynamite was caused to interrupt a radio signal which was being recorded galvanometrically, thus registering the instant of the blast. Timing was effected by a tuning fork controlling the interruption of a light beam in the usual way.

III. Rockport Granite Results

Specimen records from Rockport are reproduced in Fig. 1 and the time-distance graph is shown in Fig. 2. Velocities were obtained by least square solutions.

The recording distances of the previous work were extended to 6260 feet, leading to a revised figure for the longitudinal velocity of $16{,}840 \pm 20$ ft./sec. or 5.14 ± 0.005 km/sec.

The three-component seismograph, because of its low sensitivity, was not practicable for use throughout the investigation. It was, however, used at three different locations to give key records for the interpretation of the vertical-component records obtained elsewhere. These are shown as Nos. 3, 4 and 5 in Fig. 1. Of these, No. 4 shows the three principal phases practically

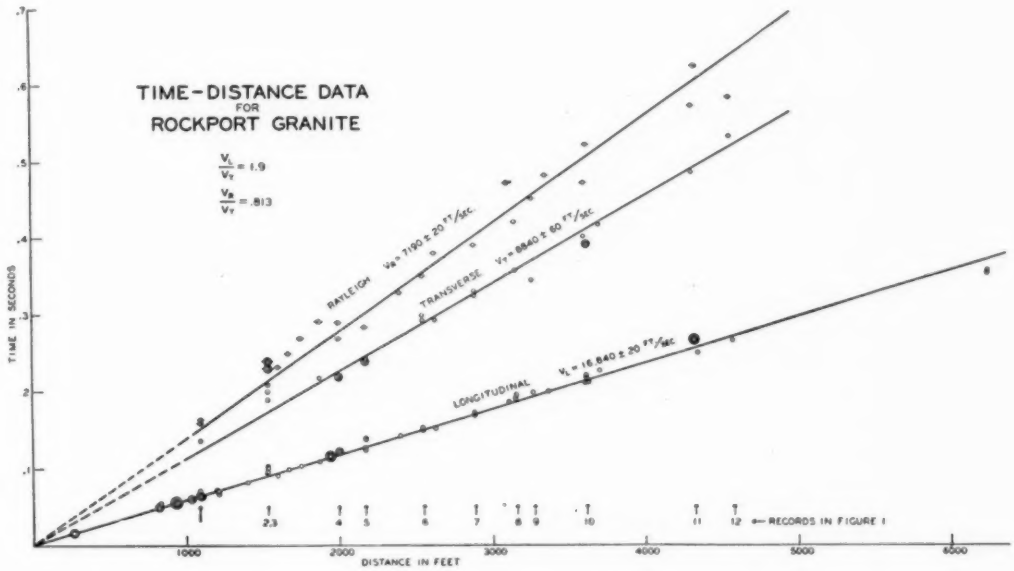

Fig. 2.

undisturbed by natural frequencies of the recording location, which confused many of the records. The component writing the top trace was oriented to record only horizontal displacements in the plane perpendicular to the line joining shot and recorder, that is, transverse to the propagation direction. The middle trace represents vertical displacements, and the bottom, longitudinal.

It may be noted that the first arrival was a compression recorded on the longitudinal and vertical components. The beginning of motion on the transverse component was accompanied by some new motion on the vertical component. This indicated the feasibility of using only a vertical component seismograph even for the transverse wave. The transverse wave was followed, closely at the short distances used, by a typical Rayleigh wave in which the ground moved, with reference to the shot point, away-up-toward-down, the retrograde sense found to be characteristic of Rayleigh waves from earthquakes.[2]

By using these three-component records as keys to the interpretation of the others, the transverse and Rayleigh waves were plot-

[2] L. D. Leet, *Empirical Investigation of Surface-Waves Generated by Distant Earthquakes*, Publ. of the Dominion Observatory **7**, No. 6, 267–322, Ottawa (1931).

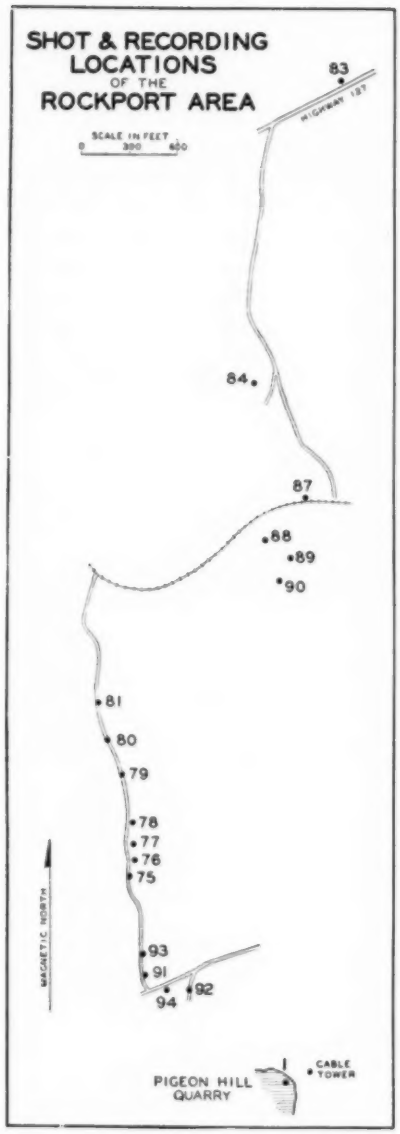
SHOT & RECORDING LOCATIONS OF THE ROCKPORT AREA
SCALE IN FEET
0 300 600
HIGHWAY 17
83
84
87
88
89
90
81
80
79
78
77
76
75
93
91
92
94
MAGNETIC NORTH
PIGEON HILL QUARRY
CABLE TOWER

B

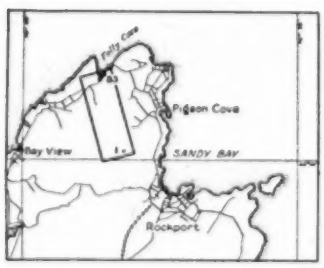
Rocky Cove
Pigeon Cove
Bay View
SANDY BAY
Rockport

A

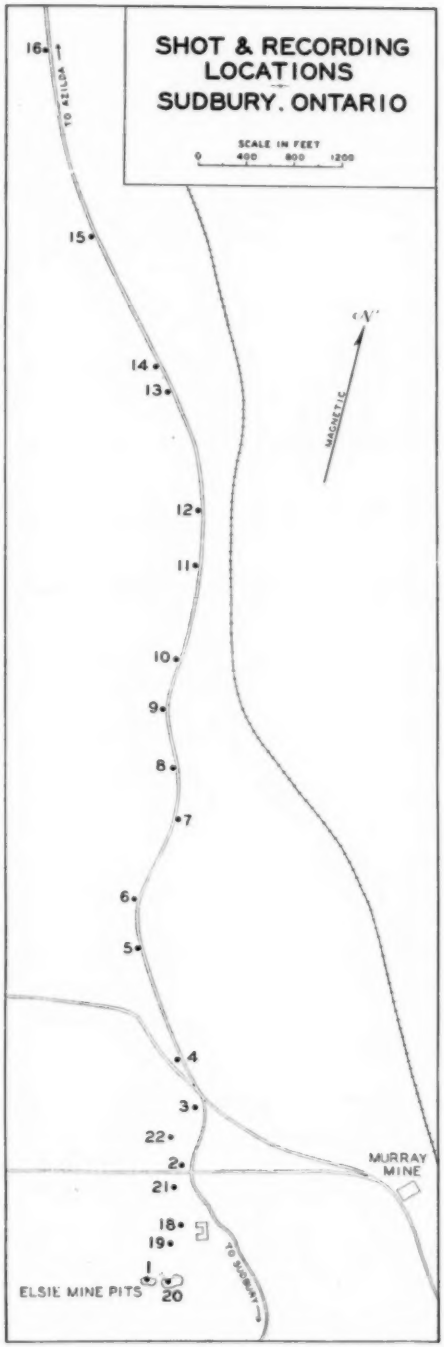
SHOT & RECORDING LOCATIONS SUDBURY, ONTARIO
SCALE IN FEET
0 400 800 1200
TO AZILDA
16
15
14
13
12
11
10
9
8
7
6
5
4
3
22
2
21
18
19
20
N
MAGNETIC
MURRAY MINE
ELSIE MINE PITS
TO SUDBURY

C

FIG. 3.

ted. The velocities were, respectively, 8840±60 ft./sec., or 2.70±0.02 km/sec., and 7190±20 ft./sec., or 2.19±0.007 km/sec.

If it is assumed that the transmitting medium obeys Hooke's law, relations between wave velocities and elastic constants of the medium may be expressed by the following equations:[3]

$$V_L=[(\lambda+2\mu)/\rho]^{\frac{1}{2}}, \quad (1)$$

$$V_T=(\mu/\rho)^{\frac{1}{2}}, \quad (2)$$

$$k=\lambda+2\mu/3, \quad (3)$$

$$\beta=1/k, \quad (4)$$

$$E=\mu(3\lambda+2\mu)/(\lambda+\mu), \quad (5)$$

$$\sigma=\lambda/2(\lambda+\mu), \quad (6)$$

where V_L is the longitudinal velocity, V_T the transverse velocity, k the bulk modulus, β the cubical compressibility, μ the rigidity, E Young's modulus, σ Poisson's ratio, and ρ the density.

The values of these constants already reported for Quincy granite[1] together with those computed for Rockport granite are listed in Table I.

TABLE I. *Elastic constants of granite and norite.*

	ρ	μ ($\times10^{-11}$ dynes/cm^2)	λ	k	E	β cm^2/dyne $\times10^{13}$	σ
Granite Quincy	2.61	1.63	3.3	4.4	4.3	22.8	0.333
Granite Rockport	2.63	1.92	3.1	4.4	5.0	22.8	0.31
Granite Average	2.62	1.78	3.2	4.4	4.7	22.8	0.32
Norite Sudbury	2.85	3.47	4.1	6.4	8.8	15.6	0.27

Several of the records of Fig. 1 show well-marked phases after the Rayleigh waves. In many cases, in fact, there appears to be an exact duplication of the first part of the record, as though there had been a double shot. Shooters have reported apparently double and sometimes triple shocks at the shot point. The possibility that these may be traceable to peculiarities of the quarry is lessened by the appearance of a similar phenomenon at Sudbury as shown on the records in Fig. 4. These later phases at both Rockport and Sudbury are as yet unexplained, and further investigation of them is proposed.

IV. Sudbury Norite Results

Copies of specimen records from Sudbury are reproduced in Fig. 4, and the time-distance graph is shown in Fig. 5. The velocities obtained from these data were:

Longitudinal = 20,400±10 ft./sec. or 6.22±0.003 km/sec.
Transverse = 11,440±20 ft./sec. or 3.49±0.006 km/sec.
Rayleigh = 9,160±30 ft./sec. or 2.79±0.01 km/sec.

A low-velocity zone was encountered in the first 1200 feet of the profile. Through the courtesy of Dr. Arthur Yates, chief geologist of the International Nickel Company, at Copper Cliff, data on this situation were obtained from a suite of thin-sections taken along a 3700-foot line northwest from the Murray Mine. Examination of these showed a sudden drop in the percentage of quartz at about the neighborhood of 1200 feet from the edge of the norite. From twenty percent, it dropped to five and less. It has been found by L. H. Adams in laboratory studies that "a decreasing silica content in rocks is accompanied by a steady decrease in compressibility,"[4] which confirms this finding of lower velocity with higher percentages of quartz.

Elastic constants of the norite, computed from velocity data, are listed in Table I. Dr. D. S. Muzzey of the Harvard Research Laboratory of Physics has obtained a comparable value for E by using a magnetostriction method to set the specimen vibrating. The mean of his values on four Sudbury norite specimens is 9.1×10^{11} dynes/cm^2.

As in the case of Rockport granite, there is a second large phase which is unexplained as yet. As nearly as its apparent beginning can be picked, it plots with a velocity of about 7550 ft./sec. or 2.30 km/sec.

[3] A. E. H. Love, *A Treatise on the Mathematical Theory of Elasticity*, Cambridge University Press, Fourth Edition, 643+ xviii pages (1927).

[4] L. H. Adams, Gerlands Beiträge zur Geophysik **31**, 315–321 (1931); also in Papers from the Geophysical Laboratory, Carnegie Institution of Washington, No. 770.

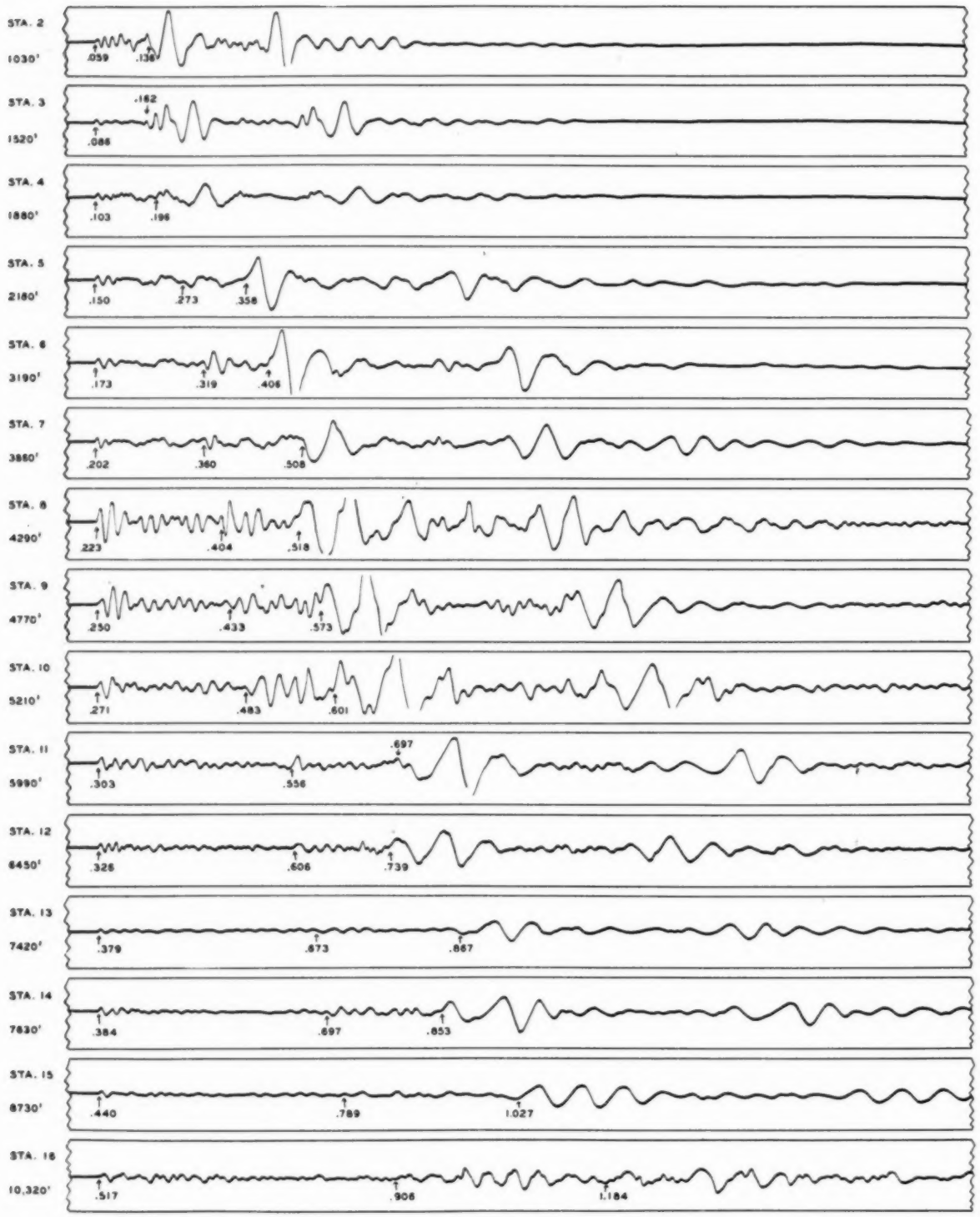

FIG. 4. Specimens of Sudbury records.

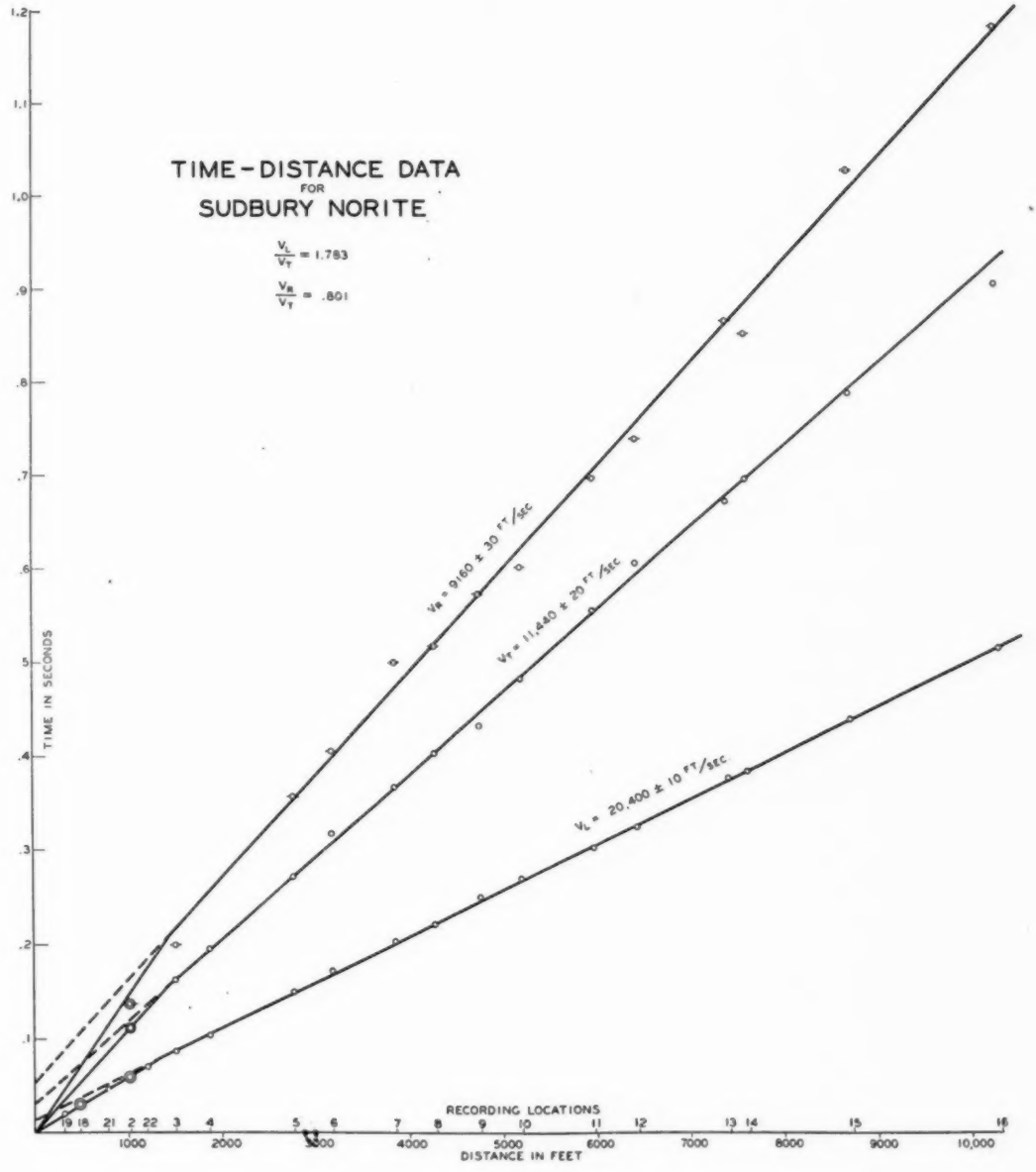
TIME-DISTANCE DATA
FOR
SUDBURY NORITE
$\frac{V_L}{V_T}$ = 1.783
$\frac{V_R}{V_T}$ = .801
V_R = 9160 ± 30 FT/SEC
V_T = 11,440 ± 20 FT/SEC
V_L = 20,400 ± 10 FT/SEC
TIME IN SECONDS
RECORDING LOCATIONS
DISTANCE IN FEET

FIG. 5.

V. Analyses and Structural Relations

Chemical and mineralogical analyses of Rockport granite have been published,[1] as have chemical analyses of Sudbury norite.[5]

The following is a mineralogical analysis of the norite, made by Dr. H. J. Fraser when a member of the Harvard University Department of Geology. Specimens were obtained through the courtesy of the International Nickel Company. Volume percentages of the constituent minerals are given in Table II.

Table II. *Volume percentages of minerals—Sudbury norite.*

	Core 1	Core 2	Core 3	Core 4
Labradorite, $Ab_{48}An_{52}$	—	67	58	70
Andesine, $Ab_{56}An_{44}$	74	—	—	—
Potash feldspar	1	1	2	4
Hypersthene (25 percent $MgSiO_3$)	15	8	18	10
Augite	3	5	4	2.5
Hornblende	2	5	8	3
Biotite	1.5	6	1.5	3
Quartz	3	8	8	6
Magnetite, apatite, sericite, kaolin, carbonate	0.5	—	0.5	1.5

Barlow,[6] Coleman[7] and Phemister[8] have published reports on the Sudbury area. Coleman's report is accompanied by a useful large-scale map, and Phemister's by a small-scale sketch of the general area. Both show the Murray and Elsie mines indicated on Fig. 3.

Because of its association with ore-bearing zones, the norite has been carefully studied in this area, and its structural relations are well known in many places. In locating contacts of the norite, we were materially aided by advance maps embodying the results of a remapping of the area which has been carried on since 1930 under the direction of the Geological Survey of Canada. For these, some excellent aerial photographs of the zone of the velocity determinations, and valuable suggestions, I am greatly indebted to Dr. W. H. Collins, Director of the Survey.

Through the further generous cooperation of Dr. Yates of the International Nickel Company, data from a number of bore-holes located approximately along our velocity profile were obtained. Fig. 6 is constructed from these, showing the dip of the bottom contact of the norite.

VI. Discussion

Attention was called in a previous report[1] to the great disparity between the elastic constants of Quincy granite computed from wave speeds observed in the field and those derived from laboratory experiments of Adams and Coker[9] at relatively low pressures. Since that time, under the direction of the Harvard Committee on Geophysical Research, Zisman has performed an elaborate series of experiments which clarify the situation. Published values of such elastic constants as Young's modulus, Poisson's ratio, and the compressibility, determined by statical methods for similar rock types, have ranged between wide limits. For granite, Young's modulus was reported by the Watertown Arsenal[10] as ranging from 3×10^{11} to 6.5×10^{11} dynes/cm^2; by Adams and Coker[9] from 4 to 6.3; by Nagaoka[11] from 1.1 to 4.2; and by Bach[12] for German granites as 2.4. The Watertown Arsenal reported Poisson's ratio for granite between 0.07 and 0.25, while Adams and Coker observed values between 0.20 and 0.26. Compressibility of granite at low pressures was reported by Adams and Coker ranging from 30.3×10^{-13} cm^2/dyne to 36.8; and

[5] Coleman, Moore, Walker, University of Toronto Studies, No. 28, p. 18 (1929).

[6] A. E. Barlow, *Origin, Geological Relations, and Composition of the Nickel and Copper Deposits of the Sudbury Mining District*, Geological Survey of Canada, Publ. No. 961, Ottawa (1907).

[7] A. P. Coleman, *The Nickel Industry: With Special Reference to the Sudbury Region, Ontario*, Canada Department of Mines, Mines Branch, Publ. No. 170, Ottawa (1913).

[8] T. C. Phemister, *Igneous Rocks of Sudbury and their Relation to the Ore Deposits*, 34th Annual Report of the Ontario Department of Mines, Vol. 34, Part VIII, Toronto (1925).

[9] F. D. Adams and E. G. Coker, Carnegie Inst. Washington, Publ. No. 46, 69 pages (1906).

[10] Watertown (Massachusetts) Arsenal Annual Report for 1895.

[11] H. Nagaoka, *Elastic Constants of Rocks and the Velocity of Seismic Waves*, Publs. of the Earthquake Investigation Committee, No. 4, 47–67, Tokyo (1900).

[12] C. Bach, *Elastizität und Festigkeit*, Fourth Edition, p. 64 (1904).

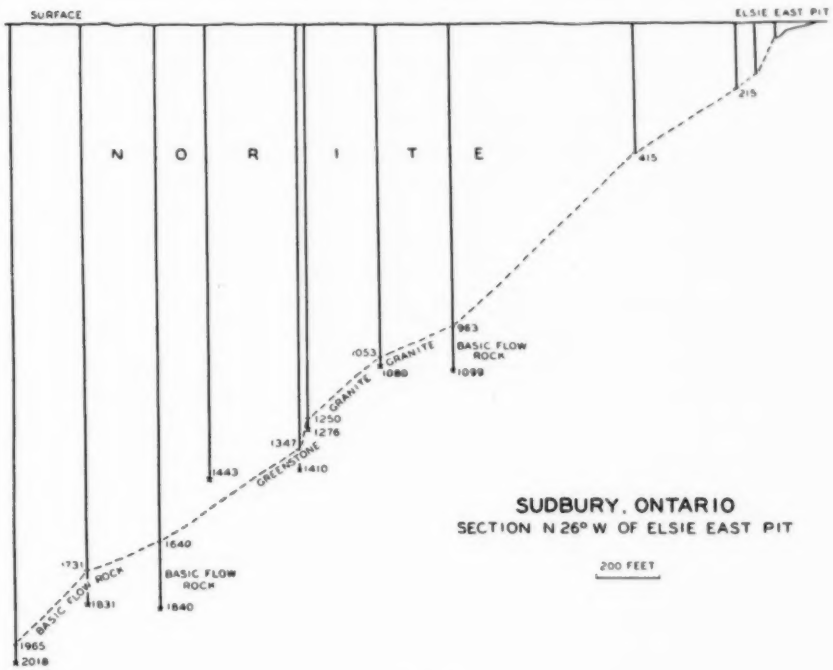

FIG. 6.

by L. H. Adams and Williamson[13] at pressures around 2000 atmospheres as 19.8 to 20.1.

Zisman,[14] working at low pressures, found for all rock types studied that Young's modulus and Poisson's ratio determined in air-dried specimens varied greatly with the mean stress used. The same was true for the compressibility of specimens covered to exclude the liquid which transmitted the pressure.[15] He pointed out, as a result, that these variations with pressure have doubtless caused much of the apparent disagreement among the results of previous experimenters, though he extended the work to show that this has not been the entire source of trouble.

Adams and Coker[9] worked for the most part with mean stresses of about 315 kg/cm². They measured the longitudinal compression and lateral extension under a unidirectional thrust, from which the compressibility was computed. Zisman, in addition to determining Young's modulus and Poisson's ratio by a similar method, measured compressibility directly under hydrostatic pressures. The only point at which approximately direct comparison is possible shows the results of these similar statical methods on Young's modulus to be somewhat variable. Zisman's figure for Young's modulus in Rockport granite, extrapolated from 202 kg/cm² mean stress to 315 kg/cm² is 7.20×10^{11} dynes/cm² whereas that of Adams and Coker for Quincy granite at the same stress was 4.64 for one specimen and 5.68 for another. Zisman, further, found that Young's modulus for Quincy granite varied greatly according to the location from which it was sampled, as had been suggested.[1] A surface specimen, for example, showed 2.13 $\times10^{11}$ dynes/cm² at a mean stress of 11.2 kg/cm² whereas one from a depth of 100 feet in a working quarry showed 5.18 at the same stress, and one at 235 feet in the same quarry, 4.85. These differences decreased with increased stresses.

Zisman established an important point regarding indirect determinations of compressi-

[13] L. H. Adams and E. D. Williamson, J. Frank. Inst. **195**, 475–529 (1923). Reprinted as No. 484 of Papers from the Geophysical Laboratory, Carnegie Inst. of Washington (1923).

[14] W. A. Zisman, *Young's Modulus and Poisson's Ratio with Reference to Geophysical Applications*, Proc. Nat. Acad. Sci. **19**, 653 (1933).

[15] W. A. Zisman, *Compressibility and Anisotropy of Rocks at and Near the Earth's Surface*, Proc. Nat. Acad. Sci. **19**, 666 (1933).

bility.[16] For Rockport granite, he found the compressibility calculated from Young's modulus and Poisson's ratio at 11.2 kg/cm² to be 66.2×10^{-13} cm²/dyne, while the value observed directly under hydrostatic pressures was 84.0. At 56.0 kg/cm² the values were 54.5 and 65.0, respectively. For Quincy granite, the figures were 70.6 as against 86.0 at 11.2 kg/cm² and 47.5 as against 67.0 at 56.0 kg/cm².

In the direct determinations of compressibility under hydrostatic pressures, all rocks when covered were found to exhibit rapid changes of compressibility with pressure until fairly well compacted (at pressures near 1000 kg/cm²). The values for Quincy and Rockport granite uncovered, on the other hand, agree well with figures of L. H. Adams and Williamson for pressures from 2000 to 10,000 atmospheres,[13] and with values computed from elastic-wave velocities. Table III compares these values. These figures are in excellent agreement as contrasted with such numbers as 91.7 for covered Rockport granite at zero pressure.

TABLE III. *Mean compressibility of granites.*

Stress kg/cm²	Laboratory determinations by direct measurement on uncovered specimens cm²/dyne$\times10^{-13}$		Computed from elastic-wave velocities
	Zisman	Adams and Williamson	
0	21.1		22.8
720	18.1		
2000		21.1	
10000		18.3	

Zisman has stated that the presence of pores and cracks explains anomalous behavior of rocks under pressure until such discontinuities are closed. It is not surprising, then, that a liquid in the openings causes the rock to possess constants found in the field, where the elastic-waves studied travel almost entirely through water-soaked materials. Accordingly, measurements of compressibility under hydrostatic pressures on liquid-soaked rocks appear to be the only available statical values at low pressures which yield seismically effective data. There is still no conclusive evidence for a fundamental difference between statically and dynamically determined elastic constants for a given rock under comparable conditions. Also, it appears that the extremely valuable law of L. H. Adams and Williamson: "the compressibility of a fresh holocrystalline rock is an additive function of the compressibility of its minerals," needs not be qualified as valid only "at moderately high pressures," but may be regarded as true for all pressures if voids are either absent or liquid-soaked.

Geological significance of granite velocities and elastic constants

Accumulating data on elastic constants and wave speeds indicate that great care needs to be exercised in attempting to use them for the identification of buried rocks, particularly near the surface.

Jeffreys adopted the symbol P_g for longitudinal waves from near-earthquakes, which show speeds averaging approximately 5.5 km/sec. In so doing, he stated, "there no longer seems to be any reason for diffidence in supposing these waves characteristic of granite." Many investigators have followed him in this and perpetuated the term "granitic layer" which, geologically, is a decidedly unfortunate generalization.

The basic criteria for identification of surface "layers" of the earth have been wave speeds and comparisons of computed elastic constants with those measured in the laboratory. Field investigations have shown now, however, that longitudinal elastic-waves have speeds of the order of 5.0 to 5.2 km/sec. in granite near the surface. On the other hand, 5.6 km/sec. has been reported by Brockamp and Wölcken[17] as the velocity of longitudinal waves in a basalt; Richards[18] found velocities of 5.18, 5.36, 5.64, 5.97, and others in that range for limestone. Similar velocities have been recognized for limestone in commercial seismic prospecting in the Gulf Coast of the United States. Preliminary results (obtained in connection with the present

[16] W. A. Zisman, *Comparison of the Statically and Seismologically Determined Elastic Constants of Rocks*, Proc. Nat. Acad. Sci. **19**, 680 (1933).

[17] Brockamp and Wölcken, Zeits. f. Geophysik **5**, 163–171 (1929).

[18] T. C. Richards, Proc. Phys. Soc. **45**, 70–81 (1933).

investigation) of an incomplete profile in a slate in Pennsylvania indicate a longitudinal velocity of the order of 6 km/sec. Zisman's results show a compressibility for Pennsylvania limestone exactly the same as that for one surface specimen of Quincy granite, and the compressibility of a quartzitic sandstone only about ten percent greater. Richards got 22.8×10^{-13} cm^2/dyne for the compressibility of one of his limestones.

The new facts are serving rather to complicate than to clarify the situation at present. The ambiguity of current lithological interpretations of velocities and seismically effective elastic constants is looming larger at every turn. It cannot be said that a longitudinal wave speed of 5.5 km/sec. is unique for granite, or even necessarily suggestive of granite. There is as yet no seismological justification for the identification of any "layer" of the earth's crust as either sedimentary or granitic.

VII. Acknowledgments

The investigations were conducted by the Harvard Seismograph Station during the summers of 1931 and 1932. The costs were met jointly by the Milton Fund of Harvard University and by the Harvard Committee for Geophysical Research. Acknowledgment has been made in the text of the valuable aid of Drs. E. L. DeGolyer, Arthur Yates, H. J. Fraser, and W. H. Collins.